Aus der Klinik und Poliklinik für Frauenheilkunde und Geburtshilfe
Klinikum der Ludwig-Maximilians-Universität München

Development and validation of gene signatures predicting the prognosis for serous ovarian cancer patients

Dissertation
zum Erwerb des Doktorgrades der Medizin
an der Medizinischen Fakultät der
Ludwig-Maximilians-Universität München

vorgelegt von
MINGJUN ZHENG
aus
Anhui,China

Jahr
2023

Mit Genehmigung der Medizinischen Fakultät der

Ludwig-Maximilians-Universität zu München

Erster Gutachter:	Prof. Dr. rer. nat. Udo Jeschke
Zweiter Gutachter:	Prof. Dr. med. Doris Mayr
Dritter Gutachter:	Prof. Dr. med. Miriam Lenhard

Mitbetreuung durch den promovierten Mitarbeiter:	Dr. med. Till Kaltofen
Dekan:	Prof. Dr. med. Thomas Gudermann

Tag der mündlichen Prüfung: 10.08.2023

Affidavit

Affidavit

Zheng, Mingjun
Surname, first name

Maistraße 11
Street

80337, München, Deutschland
Zip code, town, country

I hereby declare, that the submitted thesis entitled:

Development and validation of gene signatures predicting the prognosis for serous ovarian cancer patients

……

is my own work. I have only used the sources indicated and have not made unauthorised use of services of a third party. Where the work of others has been quoted or reproduced, the source is always given.

I further declare that the dissertation presented here has not been submitted in the same or similar form to any other institution for the purpose of obtaining an academic degree.

München, 14/08/2023
place, date

Mingjun Zheng
Signature doctoral candidate

Table of content

Affidavit **3**

Table of content **5**

List of abbreviations **6**

List of publications **8**

Your contribution to the publications **9**

1.1 Contribution to paper I 9

1.2 Contribution to paper II 9

2. Introduction **10**

2.1 Ovarian cancer 10

2.2 Tumor microenvironment (TME) 11

2.3 Immune checkpoint inhibitors 12

2.4 Lipid metabolism 13

2.5 Crosstalk between TME and lipid metabolism 15

2.6 Molecular classification and prognostic prediction model for OV 16

2.7 Aim of the present research 17

References **17**

3. Summary **22**

4. Zusammenfassung **23**

5. Paper I **24**

6. Paper II **47**

7. Acknowledgements **67**

List of abbreviations

OV	ovarian cancer
WHO	World Health Organization
EOC	epithelial ovarian cancer
SOC	serous ovarian cancer
HGSOC	high-grade serous ovarian cancer
LGSOC	low-grade serous ovarian cancer
TP53	tumor protein P53
BRCA1/2	Breast Cancer 1/2, Early Onset, Breast-Ovarian Cancer Susceptibility
KRAS	Kirsten ratsarcoma viral oncogene homolog
BRAF	v-raf murine sarcoma viral oncogene homolog B1
PARP	poly ADP-ribose polymerase
TME	tumor microenvironment,
ECM	extracellular matrix
PARP	poly ADP-ribose polymerase
FAK	focal adhesion kinase
ERK	extracellular regulated protein kinases
TAM	tumor-associated macrophages
Siglec-10	Sialic acid-binding Ig-like lectin 10
CD24	cluster of differentiation 24
DC	dendritic cell
XBP1	X-box binding protein 1
CAFs	cancer associated fibroblasts
EMT	epithelial-mesenchymal transition
EndMT	endothelial to mesenchymal transition
NK	natural killer
TCGA	The Cancer Genome Atlas
FIGO	Federation of International of Gynecologists and Obstetricians
NMF	non-negative matrix factorization
PD-1	programmed death 1

PD-L1	programmed cell death-Ligand 1
CTLA-4	cytotoxic T lymphocyte-associated antigen-4
LAG-3	Lymphocyte Activation Gene-3
TIM-3	T cell immunoglobulin and mucin domain-containing protein 3
ICIs	Immune checkpoint inhibitors
IgG	Immunoglobulin G
NADPH	Nicotinamide Adenine Dinucleotide Phosphate Hydrogen
FASN	fatty acid synthase
FABP4	fatty acid binding proteins 4
LPA	lysophosphatidicacid
VEGF	vascular endothelial growth factor
IL-8	interleukin-8
LASSO	Least absolute shrinkage and selection operator
PTGER3	prostaglandin E receptor 3
FFA	free fatty acids
CTL	cytotoxic lymphocyte
Trm	tissue- resident memory T
TIDC	tumor infiltrating dendritic cells
MGLL	monoglyceride lipase
FA	fatty acids
GEO	Gene Expression Omnibus

List of publications

1. **Zheng M**, Mullikin H, Hester A, Czogalla B, Heidegger H, Vilsmaier T, Vattai A, Chelariu-Raicu A, Jeschke U, Trillsch F, Mahner S, Kaltofen T. **Development and Validation of a Novel 11-Gene Prognostic Model for Serous Ovarian Carcinomas Based on Lipid Metabolism Expression Profile**. *International Journal of Molecular Sciences*. 2020; 21(23):9169. https://doi.org/10.3390/ijms21239169.

2. **Zheng M**, Long J, Chelariu-Raicu A, Mullikin H, Vilsmaier T, Vattai A, Heidegger HH, Batz F, Keckstein S, Jeschke U, Trillsch F, Mahner S, Kaltofen T. **Identification of a Novel Tumor Microenvironment Prognostic Signature for Advanced-Stage Serous Ovarian Cancer**. *Cancers*. 2021; 13(13):3343. https://doi.org/10.3390/cancers13133343.

3. **Zheng M**, Kessler M, Jeschke U, Mayr D, Schmoeckel E, Chelariu-Raicu A, Kolben T, Burges A, Mahner S, Trillsch F, Kaltofen T. **The necroptosis regulator RIPK3 may serve as prognostic marker in ovarian cancer.** October 2022Geburtshilfe und Frauenheilkunde 82(10)**.** Conference: 64. Kongress der Deutschen Gesellschaft für Gynäkologie und Geburtshilfe e. V. DOI: 10.1055/s-0042-1757114**.**

Your contribution to the publications

1.1 Contribution to paper I

Development and Validation of a Novel 11-Gene Prognostic Model for Serous Ovarian Carcinomas Based on Lipid Metabolism Expression Profile

As the first author of paper I, MINGJUN ZHENG performed:

Conceptualization, data curation, formal analysis, investigation, methodology, software, validation, writing—original draft.

1.2 Contribution to paper II

Identification of a Novel Tumor Microenvironment Prognostic Signature for Advanced-Stage Serous Ovarian Cancer

As the first author of paper II, MINGJUN ZHENG performed:

Conceptualization, data curation, formal analysis, investigation, methodology, validation, visualization, writing—original draft.

2. Introduction

2.1 Ovarian cancer

Ovarian cancer (OV) is a frequent female reproductive organ malignancy, with the highest death rate among three gynecological tumors [1]. According to the World Health Organization (WHO), in 2020, 314000 newly diagnosed cases of OV were reported; annually, 207000 related deaths occur worldwide due to OV, thus posing a serious threat to women's health.

Histological classification of ovarian tumors by the WHO categorizes them into sex cord-stromal, epithelial, metastatic, and germ cell tumors among which epithelial tumors are predominant, accounting for nearly 70% of all ovarian tumor cases [3]. The biological behavior of ovarian tumors with different histological types varies. Approximately 90% of ovarian malignant tumor cases are of epithelial ovarian cancer (EOC) and are mainly divided into serous ovarian cancer (SOC), endometrioid carcinoma, mucinous carcinoma, undifferentiated carcinoma, and clear cell carcinoma according to the morphology and histological structure observed under the microscope [4]. Among them, SOC is the most malignant histological type, and nearly 70% of EOC is SOC.

In 2004, Malpica et al., according to the degree of nuclear atypia and mitotic index, classified SOC into high-grade SOC (HGSOC) and low-grade SOC (LGSOC) [5]. Genetic characteristics, origin sites, and carcinogenic patterns between these grades are different, and thus, are two completely different tumor types [6-9]. The incidence rate of HGSOC accounts for 75% of EOC. As the symptoms of early onset remain undetected, more than 70% of patients are diagnosed in the advanced stage. The 10- and 5-year survival rates of patients with advanced HGSOC are only 15% and less than 30%, respectively [10]. HGSOC grow rapidly and are highly malignant and invasive, usually accompanied by TP53 and BRCA1/2 mutations [9, 11, 12]. LGSOC cases are relatively rare and often accompanied by prodromal lesions. Most of them are in the early clinical stage carrying KRAS and BRAF mutations and generally have a good prognosis [13, 14].

Surgery combined with chemotherapy based on platinum and paclitaxel is the traditional treatment for EOC. The classic cisplatin plus paclitaxel treatment scheme is effective for platinum-sensitive patients; however, 70% of EOC patients are at risk of drug resistance and recurrence [15]. With the continuous development of targeted drug molecular research, the treatment mode of EOC has gradually changed, and comprises antiangiogenic

drugs [16], poly ADP-ribose polymerase (PARP) inhibitors [17], etc., for maintenance treatment and posterior OV therapy; these have become an important part of OV treatment [17, 18]. However, EOC is highly heterogeneous, and thus, patients with the same tumor stage and pathological grade have different prognoses. Herein, we attempted to identify new markers for diagnosis and prognostic prediction of EOC patients. Our research has important clinical value for clinical diagnosis, individualized precise treatment, and prognostic prediction of EOC.

2.2 Tumor microenvironment (TME)

TME comprises extracellular matrix (ECM), tumor cells, interstitial cells surrounding the tumor cells (including immune cells, fibroblasts, adipocytes, and endothelial cells), and signaling molecules (like cytokines and chemokines) [19, 20]. Both primary TME and TME formed by distant metastasis play a crucial role in tumor cell metastasis, proliferation, invasion, drug resistance, and maintaining tumor cell stemness.

In TME, ECM (including collagen, fibronectin, laminin, etc.) can activate intracellular FAK, ERK, and other signaling pathways by binding to tumor cell surface receptors including integrin, thus enhancing tumor cell invasion, proliferation, and migration [21, 22]. The new abnormal blood vessels formed around the tumor tissue not only promote the formation of an anoxic and acidic environment around the tumor, reduce the number of immune cells, and inhibit the killing ability of immune cells against tumor cells but also limit the efficiency of drug delivery systems, thus promoting cancer [23]. Siglec-10 expressed by tumor-associated macrophages (TAMs) promote tumor cell immune escape by interacting with CD24 expressed in these cells [24]. The activation of endoplasmic reticulum stress response factor, XBP1, in dendritic cells (DCs) in TME can weaken its antigen presentation ability, resulting in loss of the ability to initiate and maintain T-cell dependent anti-tumor immunity and promoting the malignant progression of tumors [25]. As a critical component of the TME, cancer-associated fibroblasts (CAFs) can promote tumor progression by interacting with tumor cells or other TME components. Tumor cells affect the recruitment of CAFs precursors and induce epithelial cell transformation into CAFs by epithelial-mesenchymal transition (EMT) [26] or endothelial cells by endothelial-to-mesenchymal transition (EndMT) [27]. Concurrently, CAFs secrete several

growth factors, cytokines, and ECM proteins, promoting the proliferation, invasion, drug resistance, and metastasis of tumor cells, and affecting tumor prognosis [28-30].

In the early stage with ascites/peritoneal fluid, tumor cells spread through the peritoneum to form metastatic lesions, a TME feature in OV [31]. OV is a solid tumor that shows unique growth. It develops, metastasizes, and relapses in the abdominal cavity, thus forming a unique TME characterized by ascites, hypoxia, and hypoglycemia [32]. The malignant ascites in EOC patients are rich in tumor-promoting soluble factors, extracellular vesicles, exfoliated cancer cells, and different immune cells, including T cells, natural killer (NK) cells, and TAMs. The increase in ascites volume can promote the formation of a tumor-appropriate TME, thus making OV resistant to chemotherapy [33]. Compared to LGSOC patients, CAFs in the ascites of HGSOC patients are abundant and adhere to the surrounding OV cells to form spheres, thus enhancing the tumor cell adhesion ability, promoting metastasis and drug resistance, and inhibiting tumor cell apoptosis [34, 35]. Therefore, an in-depth evaluation of the molecular mechanism in TME involved in the malignant progression of EOC and TME-related early diagnostic and prognostic markers have guiding significance for clinical decision-making for these patients.

In this study, we obtained the RNA-sequencing (RNA-seq) data of SOC patients in FIGO III and IV stages from The Cancer Genome Atlas (TCGA) database. According to the expression of TME genes, the patients with advanced stage SOC were re-divided into three subtypes using the NMF algorithm. Meanwhile, we constructed an 11-gene signature based on TME genes. The signature can be used for prognostic prediction of advanced SOC and evaluating immunotherapeutic efficacy.

2.3 Immune checkpoint inhibitors

The immune checkpoint is the key to maintaining the self-tolerance of the body and protecting the tissues from self-attack after reacting to pathogens. Immune checkpoints include T-cell immunoglobulin and mucin-3 (TIM-3), PD-1 and its ligand PD-L1, lymphocyte activating gene 3 (LAG-3), and cytotoxic T-lymphocyte antigen 4 (CTLA-4) [36]. A mechanism of tumor escape from immune surveillance is the abnormal upregulation of immune checkpoint expression, which in TME can significantly inhibit the intensity and duration of immune responses [37]. The level of PD-L1 in OV increases and is related to

poor prognosis, suggesting that PD-1/PD-L1 has a key role in tumor immune responses [38].

Immune checkpoint inhibitors (ICIs) are humanized or fully humanized human immunoglobulin G (IgG) monoclonal antibodies, unlike traditional drugs that directly act on cancer cells. ICIs can activate the human immune system and target tumor cells by blocking PD-1/PD-L1 and CTLA-4/B7 signaling transduction by a specific combination [39].

The Keynote-028 study showed that the objective response rate of 26 patients with PD-L1 positive epithelial OV after receiving pabolizumab treatment was 11.5%, and the disease control rate was 34.6% [40]. Phase Ib open-label cohort study (NCT01772004) included 125 patients with refractory/recurrent OV who received avelumab treatment, showing an objective response rate of 9.7% and a disease control rate of 52% [41]. The effect of ICIs on OV patients is limited. Not all OV patients benefit from ICIs. Combination chemotherapy and targeted therapy or identifying markers that can predict the benefit of immunotherapy is a potential research direction. In this study, we used the dataset of immunotherapy genes to verify the predictive ability of the risk model based on TME-related genes for immunotherapeutic efficacy. The results showed that patients in the low-RS group had a greater likelihood of benefitting from immunotherapy.

2.4 Lipid metabolism

Abnormal metabolism is a common feature of tumors. The metabolic abnormalities of malignant tumors show the six following characteristics [42]: (1) uncontrolled glucose and amino acid uptake; (2) speculative access to nutrition; (3) synthesis of biomacromolecules and NADPH from the intermediate products of glycolysis and/or tricarboxylic acid cycle; (4) increased demand for nitrogen source; (5) metabolite driven gene expression abnormalities, and (6) metabolite interactions with the TME. Among these, abnormal lipid metabolism, especially the increase in the de novo fatty acid synthesis pathway, is implicated in the above processes.

Lipids, an important hydrophobic nutrient in the human body, include triacylglycerol, glyceryl phosphate, sterol, and sphingolipids. It plays an important role in cell membrane formation, cellular metabolism, energy storage, and signal transduction, and participates in the processes of inflammation, immunity, cellular proliferation, and cell differentiation [43, 44]. The activity and expression of enzymes participating in lipid metabolism in various tumor cells increase and the synthesis of endogenous fatty acids is enhanced [45, 46],

suggesting that abnormal lipid metabolism may serve a critical role in the development and occurrence of tumors.

Early extensive metastasis is the main feature of OV, characterized by extensive dissemination in the pelvis and abdomen and omental infiltration. Co-culture of primary human omental adipocytes with OV cells shows lipolysis of adipocytes and β-oxidation of tumor cells which provide an energy source for the growth and metastasis of OV cells [47]. Changes in lipid metabolism may occur at various stages of EOC [48]. EOC cells take up lipids in several ways to meet the high energy requirements during cell growth and signaling changes during carcinogenesis. Studies have shown that genes involved in endogenous lipid metabolism and cholesterol biosynthesis are downregulated in OV cells, indicating that in the presence of primary adipocytes, OV cells rely more on the uptake of exogenous lipids and cholesterol than on the endogenous synthesis of fatty acids [49]. Several lipid metabolism pathways, especially those related to fatty acid biosynthesis and phospholipid and its enzyme system, are closely associated with the malignant progression of OV. Fatty acid synthase (FASN), the key regulator of endogenous fatty acid synthesis, is overexpressed in OV, and its high expression is related to drug resistance and poor prognosis of these patients [50-52]. For platinum-resistant OV cells, inhibition of FASN can reduce the level of fatty acid metabolism, and combination with platinum drugs can inhibit the β-oxidation of fatty acids, jointly promoting tumor cell apoptosis [52]. Fatty acid binding protein 4 (FABP4) overexpressed at the adipocyte tumor cell interface in the OV cell membrane, functions as an intracellular lipid chaperone. Inhibition of FABP4 can reduce lipid accumulation in OV cells and invasion of tumor cells mediated by omental adipocytes [47, 53]. Lysophosphatidic acid (LPA) is a growth factor-like phospholipid produced by OV cells and mesothelial cells secreted into the peritoneal cavity. It is highly expressed in ascites of OV patients and can promote tumor angiogenesis by inducing the secretion of angiogenic factors including IL-8 and vascular endothelial growth factor (VEGF) [55]. LPA can also activate the downstream Ga12/13/RhoA signaling pathway through the LPA-1 receptor and LPA-2 receptor to induce the phosphorylation of ERM protein, thus promoting the metastasis of OV cells [56]. The development and occurrence of tumors are accompanied by several lipid-related gene changes and assessing the changes in lipid metabolism may provide a novel target for the treatment of OV.

Herein, we clustered the RNA-seq data of SOC patients from TCGA database into two subtypes (C1 and C2) according to lipid metabolism-related genes using the NMF algorithm, and the prognosis of the C2 subtype was found to be significantly better than that of the C1 subtype. Furthermore, an 11-gene signature was constructed using the Least absolute shrinkage and selection operator (LASSO) regression, which could predict the prognoses of SOC patients and guide clinical decision-making. The hub gene in the model, PTGER3, was also verified using paraffin-embedded tissue samples from clinical OV patients. The level of PTGER3 expression in the high-risk scoring group was significantly higher compared to the low-RS group. PTGER3, or EP3, is a G protein-coupled receptor. PTGER3 is widely present across various tissues and organs and participates in different pathological and physiological processes in the body, including the regulation of anticoagulation and contraction of the uterine muscle layer in early pregnancy [57]. To date, the mechanism underlying the role of PTGER3 in lipid metabolism remains unclear, but research shows that compared to M2 macrophages, the expression of PTGER3 in M1 type macrophages is up-regulated in the placenta of patients with recurrent abortion during early pregnancy [58]. Thus, lipid metabolism and TME are inextricably linked, and the role of their interaction in tumor progression needs further investigation.

2.5 Crosstalk between TME and lipid metabolism

TME has a non-immune microenvironment dominated by fibroblasts and tumor cells and an immune microenvironment dominated by immune cells [59]. Abnormal lipid metabolism can affect tumor progression and immune responses simultaneously. The proliferation of tumor cells requires massive amounts of lipids for the synthesis of cell membranes and organelles. Tumor cells can promote the exogenous uptake of lipids by up-regulating lipid transport-related proteins, enhance endogenous synthesis by regulating lipid production pathways, and secrete lipids by activating fat cells. Besides serving as the basic structural component and important energy source of immune cells, lipids also affect the proliferation and differentiation of immune cells and immune responses to tumor cells [60].

Fatty acid and lipid accumulation exert different effects on different immune cells. Fatty acid accumulation in TME can induce the loss of immune functions in more than 8 kinds of immune cells with anti-tumor effects, which is more conducive to the survival of tumor cells. Studies have shown that excessive levels of free fatty acids (FFA) can inhibit CTL-mediated tumor cell killing, and this inhibition can be restored by reducing the level of FFAs [61]. Tissue-resident memory (TRM) T cells maintain cell survival by consuming

exogenous FFAs, thus participating in anti-tumor responses [62-64]. Lipid aggregation usually leads to immunosuppression. DC is an antigen-presenting cell necessary for initiating and maintaining T-cell-dependent anti-tumor immunity. Activation of FASN in OV cells can lead to abnormal lipid accumulation and tumor-infiltrating DCs (TIDCs) to damage the activation of T cells due to excessive lipid intake [65, 66]. Different FA uptake types show differential effects on anti-tumor immune responses of macrophages. Some studies have shown that lipid accumulation occurs in macrophages from mice overexpressing monoglyceride lipase (MGLL), and these macrophages preferentially polarize to the M1-type in response to cancer-specific stimuli [67]. The enrichment of long-chain omega-3 (ω-3) FA can significantly inhibit the polarization and secretion functions of M2 macrophages in the mouse prostate tumor model [68, 69]. Therefore, crosstalk between TME and lipid metabolism exists. The demand of tumor cells for lipids increases their amount in TME, while lipid-rich TME further affects the phenotype and function of tumor-infiltrating immune cells [70]. Therefore, assessing changes in the lipid metabolism of immune cells in TME may provide new ideas for developing new and effective anti-tumor methods.

2.6 Molecular classification and prognostic prediction model for OV

The expression profiling of OV was obtained from TCGA, which can be divided into the following four subtypes: immunoreactivity, proliferation, differentiation, and interstitial [71]. Each subtype reflects different levels and patterns of immune cell infiltration. In clinical practice, patients belonging to the interstitial subtype are few, and immune-reactive, value-added, and differentiated subtypes are the most common [72]. Gene expression profiles can be used to identify prognosis-related genes in various cancer types [73, 74]. However, the gene expression profile is unsuitable for judging the prognosis of patients in clinical practice, because it requires the sequencing of fresh frozen tissues, detection of a large number of genes, and complex statistical analysis, incurring a high cost economically with poor repeatability of sequencing results. Therefore, developing a prognostic model for routine analysis like immunohistochemistry is of significance.

With the development of high-throughput sequencing technologies and the wide application of bioinformatics, many large cancer databases, including GEO and TCGA, provide researchers with the possibility to analyze large-scale gene expression data. For example, Wang et al. clustered OV patients into two subtypes using necroptosis-related genes and

constructed a 5-gene signature. There was a significant difference in the prognoses between high-risk groups [75]. Feng et al. used ferroptosis and iron metabolism-related genes to identify differentially expressed lncRNAs related to prognosis and build a prognostic model which could predict prognoses and treatment responses of OV patients [76]. The 8-gene prognostic model constructed by Bi et al. using glycolysis-related genes could predict the prognosis of OV patients and their immune responses [77]. In this study, unlike in other signatures [78-80], the 11-gene signature constructed using TME-related genes showed the best performance in a period of more than 60 months, indicating that our risk model was not only suitable for predicting the survival of patients over five years but was also a better predictor for a period fewer than 60 months. Based on lipid metabolism-related genes, we re-clustered OV patients into two subtypes (C1 and C2). The prognosis of the C2 subtype was significantly better relative to the C1 subtype. By comparing the immune scores of six different lymphocytes between the two subtypes, the median immune score of six lymphocytes in C1 was found to be significantly higher than that of the C2 subtype. Therefore, we reasonably speculated that lipid metabolism-related genes may affect the prognosis of OV patients by remodeling TME.

2.7 Aim of the present research

The purpose of this doctoral thesis was to identify new markers for predicting the prognosis and immunotherapeutic efficacy of SOC. Manuscript 1 aimed to utilize lipid metabolism-related genes to divide OV patients into two subtypes. The prognosis of patients with the C1 subtype was significantly poor relative to that of the patients with the C2 subtype. The lipid metabolism-related genes were further used to construct an 11-gene signature, which can predict the prognosis of OV patients. Manuscript 2 aimed to use TME-related genes to construct an 11-gene signature, and the risk signature can not only predict the prognosis, but also the efficacy of PD-1 immunotherapy in patients with advanced SOC.

References

1. Siegel, R.L., et al., *Cancer statistics, 2022.* CA Cancer J Clin, 2022. **72**(1): p. 7-33.
2. Sung, H., et al., *Global Cancer Statistics 2020: GLOBOCAN Estimates of Incidence and Mortality Worldwide for 36 Cancers in 185 Countries.* CA Cancer J Clin, 2021. **71**(3): p. 209-249.
3. Meinhold-Heerlein, I., et al., *The new WHO classification of ovarian, fallopian*

tube, and primary peritoneal cancer and its clinical implications. Arch Gynecol Obstet, 2016. **293**(4): p. 695-700.
4. Armstrong, D.K., et al., *NCCN Guidelines(R) Insights: Ovarian Cancer, Version 3.2022.* J Natl Compr Canc Netw, 2022. **20**(9): p. 972-980.
5. Malpica, A., et al., *Grading ovarian serous carcinoma using a two-tier system.* Am J Surg Pathol, 2004. **28**(4): p. 496-504.
6. Romero, I., et al., *Morphological and molecular heterogeneity of epithelial ovarian cancer: Therapeutic implications.* EJC Suppl, 2020. **15**: p. 1-15.
7. Zhu, S., et al., *Genomic and TCR profiling data reveal the distinct molecular traits in epithelial ovarian cancer histotypes.* Oncogene, 2022. **41**(22): p. 3093-3103.
8. Matsuo, K., et al., *Evolving population-based statistics for rare epithelial ovarian cancers.* Gynecol Oncol, 2020. **157**(1): p. 3-11.
9. Vang, R., M. Shih Ie, and R.J. Kurman, *Ovarian low-grade and high-grade serous carcinoma: pathogenesis, clinicopathologic and molecular biologic features, and diagnostic problems.* Adv Anat Pathol, 2009. **16**(5): p. 267-82.
10. Torre, L.A., et al., *Ovarian cancer statistics, 2018.* CA Cancer J Clin, 2018. **68**(4): p. 284-296.
11. Singer, G., et al., *Patterns of p53 mutations separate ovarian serous borderline tumors and low- and high-grade carcinomas and provide support for a new model of ovarian carcinogenesis: a mutational analysis with immunohistochemical correlation.* Am J Surg Pathol, 2005. **29**(2): p. 218-24.
12. Prat, J., *Ovarian carcinomas: five distinct diseases with different origins, genetic alterations, and clinicopathological features.* Virchows Arch, 2012. **460**(3): p. 237-49.
13. Singer, G., et al., *Mutations in BRAF and KRAS characterize the development of low-grade ovarian serous carcinoma.* J Natl Cancer Inst, 2003. **95**(6): p. 484-6.
14. Matsuo, K., et al., *Diagnosis-shift between low-grade serous ovarian cancer and serous borderline ovarian tumor: A population-based study.* Gynecol Oncol, 2020. **157**(1): p. 21-28.
15. Grunewald, T. and J.A. Ledermann, *Targeted Therapies for Ovarian Cancer.* Best Pract Res Clin Obstet Gynaecol, 2017. **41**: p. 139-152.
16. Monk, B.J., L.E. Minion, and R.L. Coleman, *Anti-angiogenic agents in ovarian cancer: past, present, and future.* Ann Oncol, 2016. **27 Suppl 1**: p. i33-i39.
17. George, A., S. Kaye, and S. Banerjee, *Delivering widespread BRCA testing and PARP inhibition to patients with ovarian cancer.* Nat Rev Clin Oncol, 2017. **14**(5): p. 284-296.
18. Alvarez Secord, A., et al., *Rationale for combination PARP inhibitor and antiangiogenic treatment in advanced epithelial ovarian cancer: A review.* Gynecol Oncol, 2021. **162**(2): p. 482-495.
19. Kulbe, H., et al., *A dynamic inflammatory cytokine network in the human ovarian cancer microenvironment.* Cancer Res, 2012. **72**(1): p. 66-75.
20. Bejarano, L., M.J.C. Jordao, and J.A. Joyce, *Therapeutic Targeting of the Tumor Microenvironment.* Cancer Discov, 2021. **11**(4): p. 933-959.
21. Pickup, M.W., J.K. Mouw, and V.M. Weaver, *The extracellular matrix modulates the hallmarks of cancer.* EMBO Rep, 2014. **15**(12): p. 1243-53.
22. Cox, T.R., *The matrix in cancer.* Nat Rev Cancer, 2021. **21**(4): p. 217-238.
23. Zhou, Q., et al., *Tumor extravasation and infiltration as barriers of nanomedicine for high efficacy: The current status and transcytosis strategy.* Biomaterials, 2020. **240**: p. 119902.
24. Barkal, A.A., et al., *CD24 signalling through macrophage Siglec-10 is a target for cancer immunotherapy.* Nature, 2019. **572**(7769): p. 392-396.

25. Cubillos-Ruiz, J.R., et al., *ER Stress Sensor XBP1 Controls Anti-tumor Immunity by Disrupting Dendritic Cell Homeostasis.* Cell, 2015. **161**(7): p. 1527-38.
26. Giannoni, E., et al., *Reciprocal activation of prostate cancer cells and cancer-associated fibroblasts stimulates epithelial-mesenchymal transition and cancer stemness.* Cancer Res, 2010. **70**(17): p. 6945-56.
27. Clere, N., S. Renault, and I. Corre, *Endothelial-to-Mesenchymal Transition in Cancer.* Front Cell Dev Biol, 2020. **8**: p. 747.
28. Gao, M.Q., et al., *Human breast cancer-associated fibroblasts enhance cancer cell proliferation through increased TGF-alpha cleavage by ADAM17.* Cancer Lett, 2013. **336**(1): p. 240-6.
29. Liu, T., et al., *Cancer-associated fibroblasts: an emerging target of anti-cancer immunotherapy.* J Hematol Oncol, 2019. **12**(1): p. 86.
30. Ding, H., et al., *Role of Cancer-Associated fibroblast in the pathogenesis of ovarian Cancer: Focus on the latest therapeutic approaches.* Int Immunopharmacol, 2022. **110**: p. 109052.
31. Greppi, M., et al., *Strengthening the AntiTumor NK Cell Function for the Treatment of Ovarian Cancer.* Int J Mol Sci, 2019. **20**(4).
32. Emmings, E., et al., *Targeting Mitochondria for Treatment of Chemoresistant Ovarian Cancer.* Int J Mol Sci, 2019. **20**(1).
33. Kipps, E., D.S. Tan, and S.B. Kaye, *Meeting the challenge of ascites in ovarian cancer: new avenues for therapy and research.* Nat Rev Cancer, 2013. **13**(4): p. 273-82.
34. Gao, Q., et al., *Heterotypic CAF-tumor spheroids promote early peritoneal metastatis of ovarian cancer.* J Exp Med, 2019. **216**(3): p. 688-703.
35. Wessolly, M., et al., *CAF-Associated Paracrine Signaling Worsens Outcome and Potentially Contributes to Chemoresistance in Epithelial Ovarian Cancer.* Front Oncol, 2022. **12**: p. 798680.
36. Sharma, P., et al., *The Next Decade of Immune Checkpoint Therapy.* Cancer Discov, 2021. **11**(4): p. 838-857.
37. Zhang, L., et al., *Intratumoral T cells, recurrence, and survival in epithelial ovarian cancer.* N Engl J Med, 2003. **348**(3): p. 203-13.
38. Brahmer, J.R., et al., *Safety and activity of anti-PD-L1 antibody in patients with advanced cancer.* N Engl J Med, 2012. **366**(26): p. 2455-65.
39. de Miguel, M. and E. Calvo, *Clinical Challenges of Immune Checkpoint Inhibitors.* Cancer Cell, 2020. **38**(3): p. 326-333.
40. Ott, P.A., et al., *T-Cell-Inflamed Gene-Expression Profile, Programmed Death Ligand 1 Expression, and Tumor Mutational Burden Predict Efficacy in Patients Treated With Pembrolizumab Across 20 Cancers: KEYNOTE-028.* J Clin Oncol, 2019. **37**(4): p. 318-327.
41. Disis, M.L., et al., *Efficacy and Safety of Avelumab for Patients With Recurrent or Refractory Ovarian Cancer: Phase 1b Results From the JAVELIN Solid Tumor Trial.* JAMA Oncol, 2019. **5**(3): p. 393-401.
42. Pavlova, N.N., J. Zhu, and C.B. Thompson, *The hallmarks of cancer metabolism: Still emerging.* Cell Metab, 2022. **34**(3): p. 355-377.
43. Fahy, E., et al., *Lipid classification, structures and tools.* Biochim Biophys Acta, 2011. **1811**(11): p. 637-47.
44. Swinnen, J.V., K. Brusselmans, and G. Verhoeven, *Increased lipogenesis in cancer cells: new players, novel targets.* Curr Opin Clin Nutr Metab Care, 2006. **9**(4): p. 358-65.
45. Huo, X., et al., *Landscape of the oncogenic role of fatty acid synthase in human tumors.* Aging (Albany NY), 2021. **13**(23): p. 25106-25137.

46. Fhu, C.W. and A. Ali, *Fatty Acid Synthase: An Emerging Target in Cancer.* Molecules, 2020. **25**(17).
47. Nieman, K.M., et al., *Adipocytes promote ovarian cancer metastasis and provide energy for rapid tumor growth.* Nat Med, 2011. **17**(11): p. 1498-503.
48. Niemi, R.J., et al., *Ovarian tumours of different histologic type and clinical stage induce similar changes in lipid metabolism.* Br J Cancer, 2018. **119**(7): p. 847-854.
49. Ladanyi, A., et al., *Adipocyte-induced CD36 expression drives ovarian cancer progression and metastasis.* Oncogene, 2018. **37**(17): p. 2285-2301.
50. Ji, Z., et al., *Deregulation of Lipid Metabolism: The Critical Factors in Ovarian Cancer.* Front Oncol, 2020. **10**: p. 593017.
51. Menendez, J.A. and R. Lupu, *Fatty acid synthase and the lipogenic phenotype in cancer pathogenesis.* Nat Rev Cancer, 2007. **7**(10): p. 763-77.
52. Papaevangelou, E., et al., *The effect of FASN inhibition on the growth and metabolism of a cisplatin-resistant ovarian carcinoma model.* Int J Cancer, 2018. **143**(4): p. 992-1002.
53. Gharpure, K.M., et al., *FABP4 as a key determinant of metastatic potential of ovarian cancer.* Nat Commun, 2018. **9**(1): p. 2923.
54. Mukherjee, A., et al., *Adipocyte-Induced FABP4 Expression in Ovarian Cancer Cells Promotes Metastasis and Mediates Carboplatin Resistance.* Cancer Res, 2020. **80**(8): p. 1748-1761.
55. Yu, X., Y. Zhang, and H. Chen, *LPA receptor 1 mediates LPA-induced ovarian cancer metastasis: an in vitro and in vivo study.* BMC Cancer, 2016. **16**(1): p. 846.
56. Park, J., et al., *LPA-induced migration of ovarian cancer cells requires activation of ERM proteins via LPA1 and LPA2.* Cell Signal, 2018. **44**: p. 138-147.
57. Kotani, M., et al., *Structural organization of the human prostaglandin EP3 receptor subtype gene (PTGER3).* Genomics, 1997. **40**(3): p. 425-34.
58. Ye, Y., et al., *Prostaglandin E2 receptor 3 promotes M1 macrophages polarization in unexplained recurrent pregnancy loss.* Biol Reprod, 2022. **106**(5): p. 910-918.
59. Anderson, N.M. and M.C. Simon, *The tumor microenvironment.* Curr Biol, 2020. **30**(16): p. R921-R925.
60. Kaymak, I., et al., *Immunometabolic Interplay in the Tumor Microenvironment.* Cancer Cell, 2021. **39**(1): p. 28-37.
61. Kleinfeld, A.M. and C. Okada, *Free fatty acid release from human breast cancer tissue inhibits cytotoxic T-lymphocyte-mediated killing.* J Lipid Res, 2005. **46**(9): p. 1983-90.
62. Lin, R., et al., *Fatty Acid Oxidation Controls CD8(+) Tissue-Resident Memory T-cell Survival in Gastric Adenocarcinoma.* Cancer Immunol Res, 2020. **8**(4): p. 479-492.
63. Pan, Y., et al., *Survival of tissue-resident memory T cells requires exogenous lipid uptake and metabolism.* Nature, 2017. **543**(7644): p. 252-256.
64. Stolley, J.M. and D. Masopust, *Tissue-resident memory T cells live off the fat of the land.* Cell Res, 2017. **27**(7): p. 847-848.
65. Jiang, L., et al., *Ovarian Cancer-Intrinsic Fatty Acid Synthase Prevents Anti-tumor Immunity by Disrupting Tumor-Infiltrating Dendritic Cells.* Front Immunol, 2018. **9**: p. 2927.
66. Siddiqui, S. and R. Glauben, *Fatty Acid Metabolism in Myeloid-Derived Suppressor Cells and Tumor-Associated Macrophages: Key Factor in Cancer Immune Evasion.* Cancers (Basel), 2022. **14**(1).
67. Xiang, W., et al., *Monoacylglycerol lipase regulates cannabinoid receptor 2-dependent macrophage activation and cancer progression.* Nat Commun, 2018.

9(1): p. 2574.
68. Liang, P., et al., *Effect of dietary omega-3 fatty acids on castrate-resistant prostate cancer and tumor-associated macrophages.* Prostate Cancer Prostatic Dis, 2020. **23**(1): p. 127-135.
69. Shan, K., et al., *Resolvin D1 and D2 inhibit tumour growth and inflammation via modulating macrophage polarization.* J Cell Mol Med, 2020. **24**(14): p. 8045-8056.
70. Chen, H., et al., *Metabolic heterogeneity and immunocompetence of infiltrating immune cells in the breast cancer microenvironment (Review).* Oncol Rep, 2021. **45**(3): p. 846-856.
71. Cancer Genome Atlas Research, N., *Integrated genomic analyses of ovarian carcinoma.* Nature, 2011. **474**(7353): p. 609-15.
72. Tothill, R.W., et al., *Novel molecular subtypes of serous and endometrioid ovarian cancer linked to clinical outcome.* Clin Cancer Res, 2008. **14**(16): p. 5198-208.
73. De Preter, K., et al., *Accurate outcome prediction in neuroblastoma across independent data sets using a multigene signature.* Clin Cancer Res, 2010. **16**(5): p. 1532-41.
74. Ramaswamy, S., et al., *A molecular signature of metastasis in primary solid tumors.* Nat Genet, 2003. **33**(1): p. 49-54.
75. Wang, Z., et al., *Identification and Verification of Necroptosis-Related Gene Signature With Prognosis and Tumor Immune Microenvironment in Ovarian Cancer.* Front Immunol, 2022. **13**: p. 894718.
76. Feng, S., et al., *Integrated clinical characteristics and omics analysis identifies a ferroptosis and iron-metabolism-related lncRNA signature for predicting prognosis and therapeutic responses in ovarian cancer.* J Ovarian Res, 2022. **15**(1): p. 10.
77. Bi, J., et al., *Establishment of a novel glycolysis-related prognostic gene signature for ovarian cancer and its relationships with immune infiltration of the tumor microenvironment.* J Transl Med, 2021. **19**(1): p. 382.
78. Yue, H., et al., *Gene signature characteristic of elevated stromal infiltration and activation is associated with increased risk of hematogenous and lymphatic metastasis in serous ovarian cancer.* BMC Cancer, 2019. **19**(1): p. 1266.
79. Wang, L., et al., *Identifying Gene Signature for the Detection of Ovarian Cancer Based on the Achieved Related Genes.* Gynecol Obstet Invest, 2017. **82**(4): p. 361-370.
80. Sabatier, R., et al., *A seven-gene prognostic model for platinum-treated ovarian carcinomas.* Br J Cancer, 2011. **105**(2): p. 304-11.

3. Summary

The current doctoral dissertation was conducted to evaluate new markers for the prognosis of patients with SOC. For Manuscript 1, RNA sequencing data of SOC patients were obtained from the TCGA and GEO databases. SOC patients were divided into two subtypes based on lipid metabolism-related genes. Differentially expressed genes between the subtypes were significantly enriched with regard to regulation of the activation of leukocytes, T cells, lymphocytes, and other signaling pathways. Further, a signature of eleven genes including PI3, RGS, ADORA3, CH25H, CCDC80, PTGER3, MATK, KLRB1, CCL19, CXCL9, and CXCL10, was established. Real-world samples were used to confirm that PTGER3 was up-regulated in the high-RS group, as indicated by immunohistochemistry. The lipid metabolism-related gene signature may be used as a potential prognostic marker of SOC. In Manuscript 2, the multi-gene signature that was established based on TME-related genes was shown to facilitate prognosis and predict immune responses of patients with advanced SOC.

4. Zusammenfassung

Diese Dissertation wurde durchgeführt um neue Marker für die Prognose von Patienten mit serösem Ovarialkarzinom (SOC) zu evaluieren. Für Manuskript 1 wurden RNA-Sequenzierungsdaten von Patienten mit SOC aus den TCGA- und GEO-Datenbanken bezogen. SOC-Patienten wurden basierend auf Genen assoziiert mit dem Fettstoffwechsel in zwei Subtypen eingeteilt. Differentiell exprimierte Gene zwischen den beiden Subtypen waren signifikant angereichert hinsichtlich der Regulierung der Aktivierung von Leukozyten, T-Zellen, Lymphozyten und anderen Signalwegen. Eine 11-Gen-Signatur einschließlich PI3, RGS, ADORA3, CH25H, CCDC80, PTGER3, MATK, KLRB1, CCL19, CXCL9 und CXCL10 wurde weiter konstruiert. Patientenproben wurden verwendet, um durch immunhistochemische Färbung zu bestätigen, dass PTGER3 in der Hoch-RS-Gruppe hochreguliert war. Die fettstoffwechselbezogene Gensignatur könnte als potenzieller prognostischer Marker für SOC verwendet werden. In Manuskript 2 wird gezeigt, dass die Multi-Gen-Signatur auf der Grundlage von Tumor-Mikro-Milieu-verwandten Genen die Prognose von Patienten mit fortgeschrittenem SOC ermöglicht und deren Immunantworten vorhersagen kann.

5. Paper I

International Journal of
Molecular Sciences

MDPI

Article

Development and Validation of a Novel 11-Gene Prognostic Model for Serous Ovarian Carcinomas Based on Lipid Metabolism Expression Profile

Mingjun Zheng [1], Heather Mullikin [1], Anna Hester [1], Bastian Czogalla [1], Helene Heidegger [1], Theresa Vilsmaier [1], Aurelia Vattai [1], Anca Chelariu-Raicu [1], Udo Jeschke [1,2], Fabian Trillsch [1], Sven Mahner [1] and Till Kaltofen [1,*]

[1] Department of Obstetrics and Gynecology, University Hospital, LMU Munich, Maistrasse 11, 80337 Munich, Germany; Mingjun.Zheng@med.uni-muenchen.de (M.Z.); heather.mullikin@gmail.com (H.M.); Anna.Hester@med.uni-muenchen.de (A.H.); Bastian.Czogalla@med.uni-muenchen.de (B.C.); Helene.Heidegger@med.uni-muenchen.de (H.H.); Theresa.Vilsmaier@med.uni-muenchen.de (T.V.); Aurelia.Vattai@med.uni-muenchen.de (A.V.); Anca.Chelariuraicu@med.uni-muenchen.de (A.C.-R.); Udo.Jeschke@med.uni-muenchen.de (U.J.); Fabian.Trillsch@med.uni-muenchen.de (F.T.); Sven.Mahner@med.uni-muenchen.de (S.M.)

[2] Department of Obstetrics and Gynecology, University Hospital Augsburg, Stenglinstrasse 2, 86156 Augsburg, Germany

* Correspondence: Till.Kaltofen@med.uni-muenchen.de

Received: 19 September 2020; Accepted: 27 November 2020; Published: 1 December 2020

check for updates

Abstract: (1) Background: Biomarkers might play a significant role in predicting the clinical outcomes of patients with ovarian cancer. By analyzing lipid metabolism genes, future perspectives may be uncovered; (2) Methods: RNA-seq data for serous ovarian cancer were downloaded from The Cancer Genome Atlas and Gene Expression Omnibus databases. The non-negative matrix factorization package in programming language R was used to classify molecular subtypes of lipid metabolism genes and the limma package in R was performed for functional enrichment analysis. Through lasso regression, we constructed a multi-gene prognosis model; (3) Results: Two molecular subtypes were obtained and an 11-gene signature was constructed (PI3, RGS, ADORA3, CH25H, CCDC80, PTGER3, MATK, KLRB1, CCL19, CXCL9 and CXCL10). Our prognostic model shows a good independent prognostic ability in ovarian cancer. In a nomogram, the predictive efficiency was notably superior to that of traditional clinical features. Related to known models in ovarian cancer with a comparable amount of genes, ours has the highest concordance index; (4) Conclusions: We propose an 11-gene signature prognosis prediction model based on lipid metabolism genes in serous ovarian cancer.

Keywords: ovarian neoplasms; lipid metabolism; genes; The Cancer Genome Atlas (TCGA); Gene Expression Omnibus (GEO)

1. Introduction

Epithelial ovarian cancer (EOC) is one of the most lethal gynecological malignancies worldwide [1]. It has a high mortality, constituting 3.3% of all malignant diseases and claiming 5.6% of gynecological cancer-related deaths of women in Germany. [2]. Although the prognosis has been improved to a certain degree by surgical treatment, platinum-based chemotherapy, bevacizumab and poly ADP ribose polymerase inhibitors, the 5-year survival of patients with advanced stage EOC is poor at only 20–30% [3,4]. Therefore, when investigating new therapeutic options it is of clinical importance to identify reliable prognostic markers or models to more accurately study their role in the occurrence and development of EOC.

To date, many driver genes have already been identified. For instance, BRCA1, BRCA2, p53, KRAS, PIK3CA, CTNNB1 and PTEN can be implicated in the development of EOC [5]. EPOR is known for its biological effect on tumor growth [6], TTC30A and LRRC8D regulate the expression of host proteins [7], Tfcp2l1 may be involved in the differentiation of ovarian tumor stem cells [8] and the expression of FOXM1 is correlated with chemotherapy resistance and poor prognosis in patients with non-serous epithelial EOC [9].

Recent studies suggest that lipid metabolism disorders may represent important metabolic markers for cancer cells in general. Metabolic reprogramming, including changes in lipid metabolism, can occur in tumor cells and the tumor microenvironment and has impact on the growth, proliferation, invasion and metastasis of cancer cells [10–13]. Braicu et al. [14] conducted a comprehensive lipidomics analysis on the serum samples of 147 EOC patients and 98 control subjects with benign ovarian tumors or non-tumorous diseases. They revealed that a variety of lipid molecules could act as prognostic markers for EOC, due to their superior efficacy compared to CA125. Furthermore, EOC cells are known to be more aggressive after reprogramming lipid metabolism in an ascites microenvironment. Targeting the signal transduction axis of lipid metabolism can effectively prevent peritoneal metastasis of EOC under experimental circumstances [15]. Niemi et al. [10] showed that changes in lipid metabolism can occur in various stages of EOC and can become intensified in a consistent pattern with advanced cancer stages.

However, the role and the prognostic value of genes related to lipid metabolism in EOC remain to be clarified, since a lack of large-scale EOC sample populations, especially for validation sets, constrains the reliability and validity of previous research results. However, in an era of big data, the emergence of genome-sequencing technologies and data [16–19] may help in tumor diagnosis and prognosis prediction [20].

Accordingly, we collected genes related to lipid metabolism and constructed molecular subtypes of serous EOC based on lipid metabolism genes according to The Cancer Genome Atlas (TCGA) and the Gene Expression Omnibus (GEO) databases. After this, we established an 11-gene signature prognosis prediction model to validate its performance in a large panel of tumors.

2. Results

2.1. Molecular Subtypes of Lipid Metabolism-Related Genes

2.1.1. Identification of Two Molecular Subtypes

After preprocessing, a total of 751 lipid metabolism genes from our serous EOC samples qualified for subsequent analysis (Supplementary Table S1). We then conducted a univariable Cox analysis using the coxph function to obtain 64 prognostic genes ($p < 0.05$). The expression matrix of these genes was obtained and the TCGA samples were divided into two clusters through the non-negative matrix factorization (NMF) algorithm (Supplementary Figure S1). The levels of expression of the 64 genes in the two subtypes are shown in Figure 1a and they differ significantly between cluster 1 (C1) and cluster 2 (C2). Furthermore, the log-rank test showed a significant difference in the overall survival (OS) between these two groups ($p = 0.026$) (Figure 1b) with a better prognosis among C2: 36.82 months in C1 vs. 43.61 months in C2. When we analyzed the disease-specific survival, we were able to confirm a significant difference between both clusters ($p = 0.033$) (data not shown).

2.1.2. Relationship between Two Subtypes and Immunity

It is known that the expression of immune genes is associated with different genomic aberrations in gynecological cancers [21] and Yang et al. [22] showed the dependence of tumor-infiltrating lymphocyte type on different types of EOC. To include an immunological viewpoint on our two clusters we used the Tumor Immune Estimation Resource (TIMER) tool. We then compared the immune scores for six different lymphocytes between C1 and C2 (Figure 2, Supplementary Table S2). Overall, the median

immune scores of the six types of lymphocytes are significantly higher in the C1 than in the C2 subtype ($p < 0.01$): B cells 0.076 vs. 0.072, CD4+ T cells 0.152 vs. 0.135, CD8+ T cells 0.181 vs. 0.147, neutrophil cells 0.143 vs. 0.109, macrophages 0.072 vs. 0.053, dendritic cells 0.517 vs. 0.453.

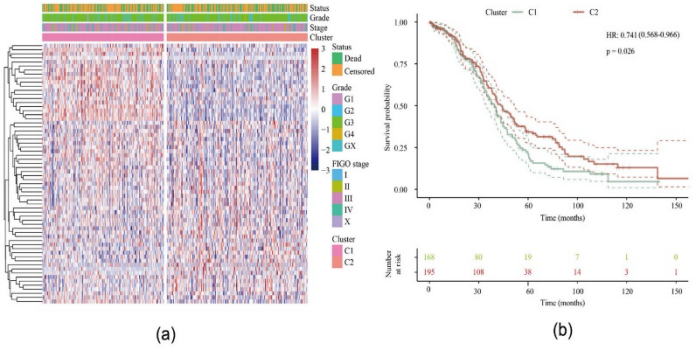

Figure 1. Identification of two molecular subtypes: (**a**) Heat map of clustering of 64 prognosis-related genes. (**b**) Survival curve of molecular subtypes including hazard ratio (HR) with 95% confidence interval (CI) and *p*-value.

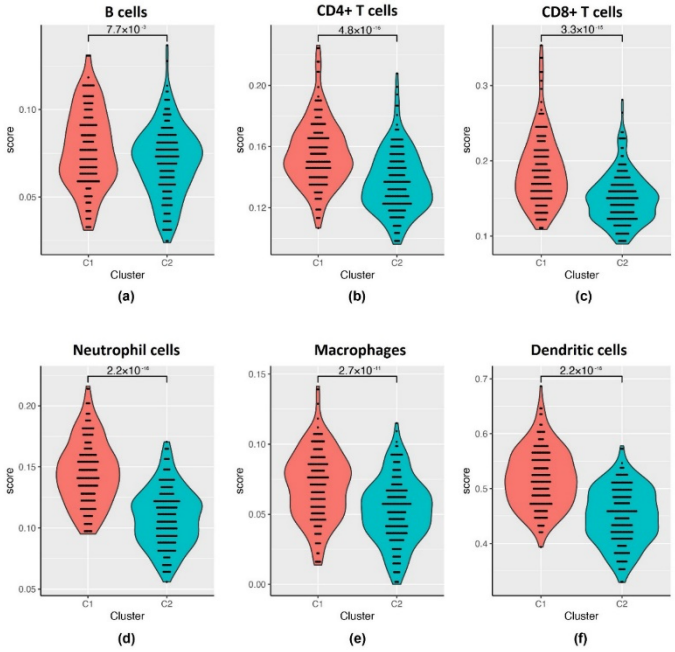

Figure 2. Tumor Immune Estimation Resource (TIMER) immune scores for cluster 1 (C1) and cluster 2 (C2) subtypes with the *p*-value in between for: (**a**) B cells; (**b**) CD4+ T cells; (**c**) CD8+ T cells; (**d**) neutrophil cells; (**e**) macrophages; (**f**) dendritic cells.

2.2. Analysis of DEGs between Subtypes

2.2.1. The DEGs in C2 Subtype Were Mainly Downregulated

A total of 925 differentially expressed genes (DEGs) between the two subtypes were identified (Supplementary Table S3). As shown in Supplementary Figure S2, in C2 subtype, 193 genes were upregulated in comparison to C1, whereas 732 genes were downregulated when compared to C1.

2.2.2. DEGs Are Enriched in Tumor-Related Pathways

We performed Kyoto Encyclopedia of Genes and Genomes (KEGG) and Gene Ontology (GO) functional enrichment analysis on these 925 DEGs using the clusterProfiler package. The DEGs were collectively enriched to 1871 biological process annotations and there were 749 significant annotations with a false discovery rate (FDR) < 0 (Supplementary Table S4a). For visualization, we selected the top ten functional annotations according to FDR. As shown in Figure 3a, genes are significantly enriched e.g., in regulation of leukocyte activation, T cell activation, regulation of lymphocyte activation and many more. Similarly, 66 significant functional annotations were enriched in the molecular function region (FDR < 0.01) and 58 significant functional annotations were enriched in the cellular component region (FDR < 0.01) (Figure 3b,c, Supplementary Table S4b,c). Under the scope of the KEGG database, DEGs were significantly enriched in 39 pathogenetic pathways, e.g., for rheumatoid arthritis or inflammatory bowel disease (Figure 3d, Supplementary Table S4d).

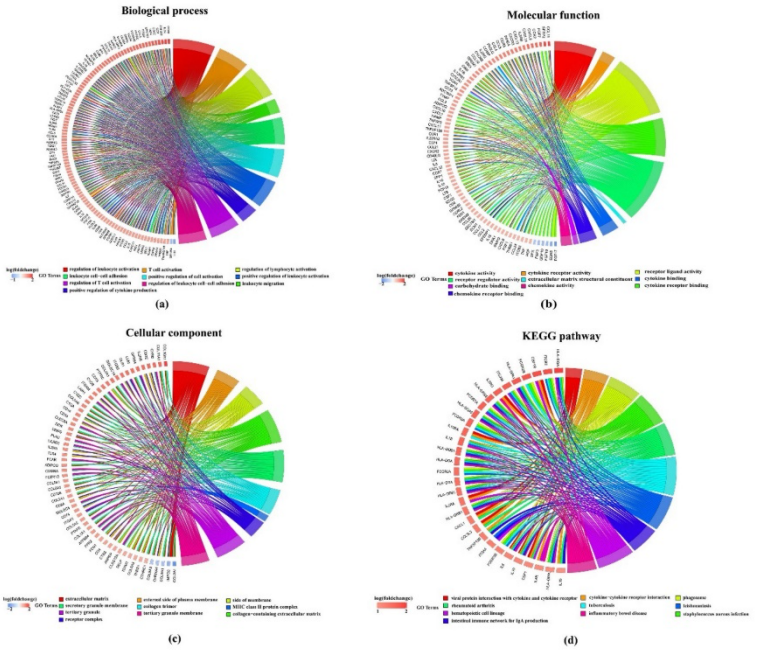

Figure 3. Kyoto Encyclopedia of Genes and Genomes (KEGG) and Gene Ontology (GO) functional enrichment analysis on 925 differentially expressed genes (DEGs) with each top ten annotations in: (**a**) Biological process subsection of GO; (**b**) molecular function subsection of GO; (**c**) cellular component subsection of GO; (**d**) KEGG pathways.

2.3. Construction of a Prognostic Risk Model

2.3.1. Randomly Grouping of Training and Testing Cohort

The final training cohort had a total of 253 samples and the testing cohort had 110 samples in total. The difference between them was analyzed using a chi-square test. The results showed that the grouping was reasonable and no significant differences were found between the groups comparing event rate, Fédération Internationale de Gynécologie et d'Obstétrique (FIGO) stage, age and grade (Table 1).

Table 1. Sample information of The Cancer Genome Atlas (TCGA) training and testing cohorts.

Clinical feature		Training Cohort	Testing Cohort	X-Squared	*p*-Value
Event	Censored	99	42	0.0028	0.9575
	Dead	154	68		
FIGO stage	I	0	1	3.9129	0.4179
	II	15	5		
	III	198	87		
	IV	37	17		
	None	3	0		
Age	≤60	132	59	0.0202	0.8870
	>60	121	51		
Grade	G1	1	0	2.7958	0.5926
	G2	29	13		
	G3	217	93		
	G4	0	1		
	None	6	3		

2.3.2. Univariable Analysis of Training Cohort

We used the training cohort to conduct a univariable analysis on each gene by using survival coxph function package. A *p*-value less than 0.05 was selected as the threshold. We found 30 prognosis-related significant DEGs (Supplementary Figure S3, Supplementary Table S5).

2.3.3. Construction of the 11-Gene Signature Using Lasso Regression

Lasso Cox regression analysis was performed to compress the 30 genes from Section 2.3.2. As seen in Supplementary Figure S4a, with decreased lambda, the number of independent variable coefficients approaching zero increased gradually. The model is optimal, which means stable, when lambda = 0.0686 (Supplementary Figure S4b). Therefore, we selected 11 genes under the condition of lambda = 0.0686 as the target genes (Supplementary Table S6): PI3, RGS1, ADORA3, CH25H, CCDC80, PTGER3, MATK, KLRB1, CCL19, CXCL9 and CXCL10. These 11 genes were analyzed by multivariate Cox analysis to obtain each coefficient.

2.3.4. Construction and Evaluation of a Risk Model

The 11-gene risk model was established according to the following formula:

$$\begin{aligned}&\text{risk score (RS)} =\\&(0.0004 * \text{expression level of PI3})\\&+(0.0044 * \text{expression level of RGS1})\\&+(0.0227 * \text{expression level of ADORA3})\\&+(0.0103 * \text{expression level of CH25H})\\&+(0.0078 * \text{expression level of CCDC80})\\&+(0.0510 * \text{expression level of PTGER3})\\&+(0.0357 * \text{expression level of MATK})\\&+(-0.0640 * \text{expression level of KLRB1})\\&+(-0.0294 * \text{expression level of CCL19})\\&+(-0.0020 * \text{expression level of CXCL9})\\&+(-0.0006 * \text{expression level of CXCL10}).\end{aligned}$$

The risk score (RS) of each sample was calculated and consequently the median RS was applied as the threshold to subdivide the training cohort into a high-risk group (HRG) and a low-risk group (LRG). Considering the overall distribution of the sample's OS, we evaluated the 2-year, 3-year and 5-year predictive effect of the model. In the receiver operating characteristic (ROC) curve the 5-year area under the curve (AUC) was 0.724 in the training cohort. We observed a significant difference in the Kaplan-Meier (KM) curve between the HRG and the LRG (Figure 4a).

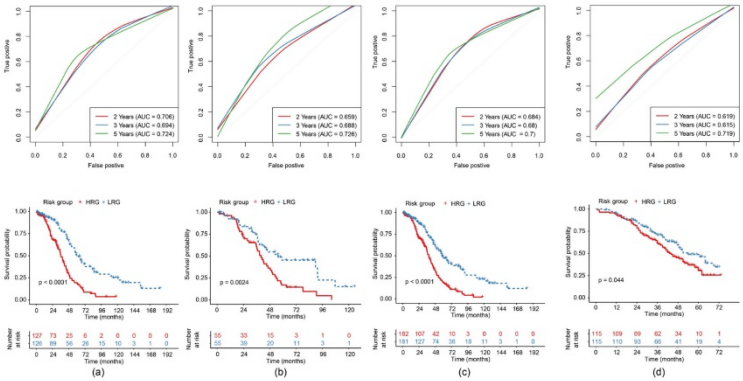

Figure 4. Construction and evaluation of the 11-gene risk model with each receiver operating characteristic (ROC) curve (area under the curve (AUC) of the 2-year, 3-year and 5-year predictive effect) above and the KM (Kaplan-Meier) curve comparing high-risk group (HRG) and low-risk group (LRG) beneath for: (**a**) TCGA training cohort; (**b**) TCGA testing cohort; (**c**) TCGA-(epithelial ovarian cancer (EOC) cohort; (**d**) GEO Series 32026 (GSE32026) cohort.

To verify the stability and reliability of the model, we also calculated the prediction performance of this model in the testing cohort for the 2-, 3- and 5-year predictive effect. The result of the testing cohort showed a 5-year AUC of 0.726 and confirmed a significant difference between the HRG and the LRG in the KM curve (Figure 4b). The results of the ROC curve analysis and the KM curve of the whole TCGA-EOC cohort (Figure 4c), as well as the independent external validation through GEO Series 32026 (GSE32026), saw identical results (Figure 4d).

Among these 11 genes, expression levels of PI3, RGS1, ADORA3, CH25H, CCDC80, PTGER3 and MATK were upregulated in the HRG compared with the LRG. In contrast, the expression levels of KLRB1, CCL19, CXCL9 and CXCL10 were upregulated in the LRG, showing a consistent pattern within the training and the validation cohorts (Supplementary Figure S5).

In order to evaluate the stability of the model, we conducted 1000 random samplings at different proportions from all the TCGA-EOC samples. We found significance in 997 out of 1000 times when the sampling ratio was 0.5 (Supplementary Figure S6). This confirmed a lower sampling bias.

2.4. Univariable and Multivariable Analysis of Gene Signature

To identify the independence of the 11-gene signature model in clinical application, we conducted univariable and multivariable Cox regression analysis to investigate the relevant hazard ratio (HR), 95% confidence interval (CI) of HR and the *p*-value. We systematically analyzed the clinical information of TCGA patients including age, FIGO stage, grade and our RS of the 11-gene signature (Table 2). Univariable Cox regression analysis found that the RS was significantly related to survival (HR = 1.593, 95% CI: 1.377-1.843, p = 3.77E-10). Moreover, the corresponding multivariable Cox regression analysis found that the RS also correlated significantly with survival (HR = 1.534, 95% CI: 1.322-1.780, p = 1.65E-08) (Supplementary Figure S7).

Table 2. Univariable and multivariable analysis of the TCGA cohort.

Clinical Feature	Univariable Analysis			Multivariable Analysis		
	HR	95% CI	*p*-Value	HR	95% CI	*p*-Value
FIGO stage	1.929	0.856–4.349	0.1130	1.705	0.742–3.917	0.2080
Age	1.186	0.791–1.778	0.4090	1.087	0.718–1.646	0.6940
Grade	1.291	0.992–1.680	0.0576	1.193	0.910–1.566	0.2020
RS	1.593	1.377–1.843	<0.001	1.534	1.322–1.780	<0.001

2.5. Survival Curves of Risk Models in Different Clinical Subgroups

In order to verify the effect of our model on clinical subgroup characteristics, we classified the TCGA-EOC cohort according to the different clinical characteristics from Table 1. Significant differences were found between the HRG and the LRG in FIGO stage III and IV ($p < 0.05$) (Figure 5a,b). Due to an insufficient amount of stage I and II samples, we did not analyze them. G1 samples were also not examined because of the lack of data. G2 sample differences between both groups were not significant (Figure 5c), whereas G3 samples showed a significant difference ($p < 0.01$) (Figure 5d). Patient samples ≤60 years as well as >60 years showed a significant difference between the HRG and the LRG ($p < 0.0001$) (Figure 5e,f).

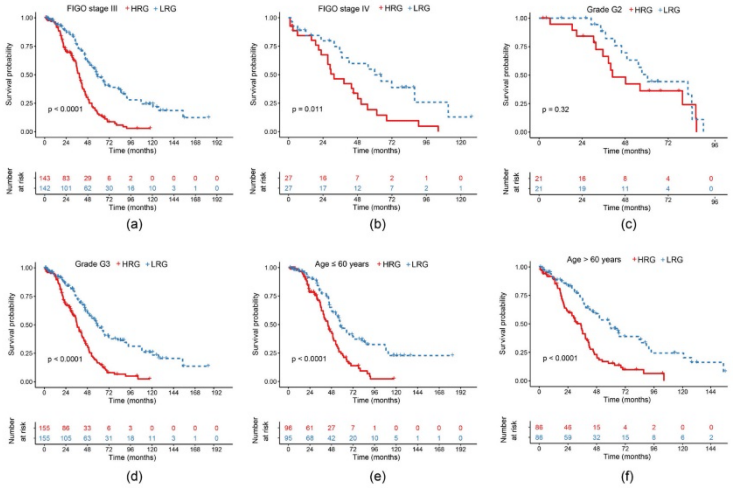

Figure 5. KM curves of overall survival (OS) of the 11-gene risk model in different clinical subgroups: (**a**) Fédération Internationale de Gynécologie et d'Obstétrique (FIGO) stage III; (**b**) FIGO stage IV; (**c**) grade G2; (**d**) grade G3; (**e**) age ≤60 years; (**f**) age >60 years.

2.6. Survival Prognosis on Different Mutation Subtypes in the Risk Model

To verify the effectiveness of our model on different common mutation subtypes of EOC, the TCGA-EOC cohort was classified according to different single nucleotide variant types. In TCGA there are a total of 436 exon sequencing samples. Here, we saw 411 altered ones (=94.27%). Mutations of TP53 and TTN dominated this classification (Figure 6a). Consequently, we conducted the KM curves for the 363 RNA-Seq samples and found that, regardless of with/without a TP53/TNN mutation, prognosis in the HRG was worse compared to the LRG (Figure 6b–e).

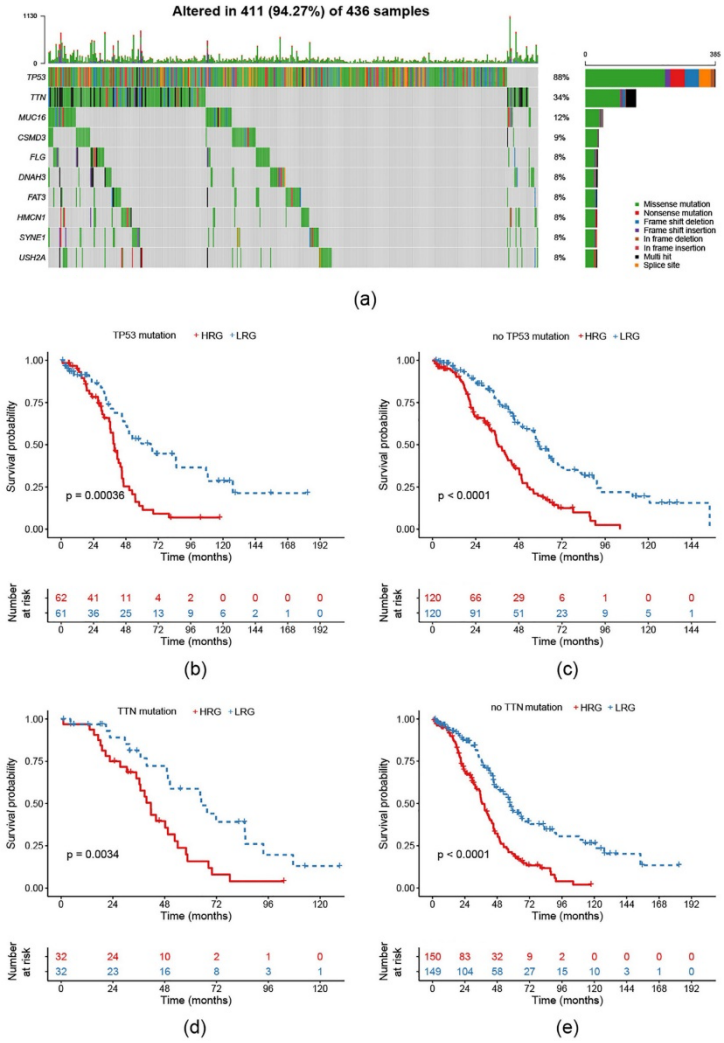

Figure 6. Analysis of the 11-gene signature model in different single nucleotide mutations: (**a**) Distribution of common single nucleotide mutations in EOC with 94.27% samples altered; (**b**) KM curve of TP53-mutated samples; (**c**) KM curve of not TP53-mutated samples; (**d**) KM curve of TTN-mutated samples; (**e**) KM curve of not TP53-mutated samples.

2.7. Construction of Nomogram Model Based on RS and Clinical Features

We combined the traditional clinical features FIGO stage, age and grade with our RS to construct a nomogram model to predict the OS of EOC patients (Figure 7a). In the modeling results the RS has the greatest impact on survival prediction. Calibration plots were used to visualize the performances

of the nomograms. The 2-year, 3-year and 5-year calibration plots demonstrated the performance of our model (Figure 7b).

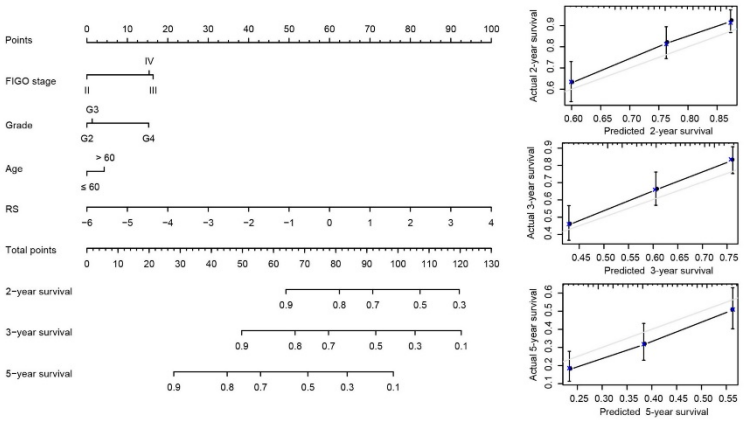

Figure 7. Construction of nomogram model: (**a**) Nomogram predicting 2-, 3- and 5-year OS for patients with EOC. The nomogram is applied by adding up the points identified on the points scale for each variable to a total points amount. Finally, beneath the total points, the probability of 2-, 3- or 5-year survival is projected on the bottom scales. (**b**) Calibration curves for nomogram predicted 2-, 3- and 5-year OS for patients with EOC in relation to actual survival.

Under consideration of the nomogram, we saw its notably superior predictive ability compared to clinical features themselves or the RS alone. The concordance index (C-index) of the nomogram was the highest (0.663) compared to the other variables, as seen in Table 3.

Table 3. Comparison of concordance indexes (C-indexes) between clinical features, risk score (RS) and nomogram.

Variables	C-Index	95% CI of C-Index	*p*-Value
FIGO stage	0.609	0.523–0.696	0.013
Age	0.619	0.547–0.690	0.001
Grade	0.593	0.508–0.678	0.032
RS	0.658	0.602–0.684	<0.001
Nomogram	0.663	0.625–0.701	<0.001

2.8. ROC Curve and DCA of Nomogram Model

To demonstrate putative advantages of the nomogram model, we compared the 2-, 3- and 5-year ROC curves of the single variables against the nomogram curve. The highest AUC each was seen for the nomogram model (Figure 8a–c). Furthermore, a decision curve analysis (DCA) confirmed our expectations. The net benefit in 2-, 3- and 5-year predictions was the highest in the combined nomogram model compared to the single variable models (Figure 8d–f). These methods showed the improved clinical utility of our nomogram model.

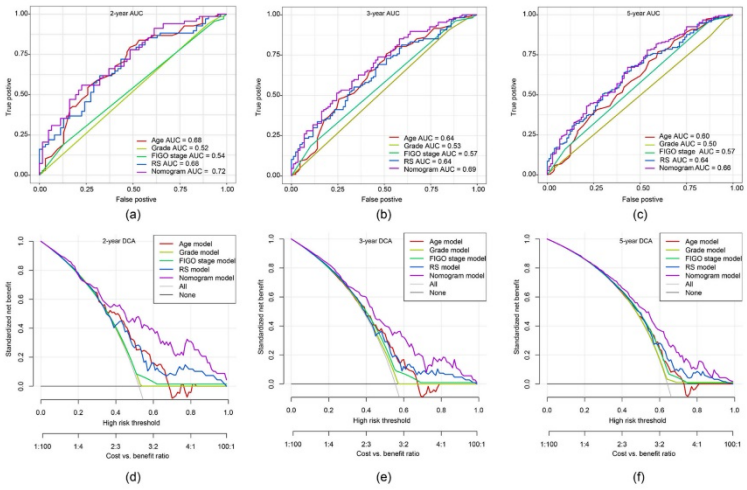

Figure 8. The time-dependent ROC curve and decision curve analysis (DCA) on the nomogram compared to single variable models. Through the ROC curves the accuracy of the models was tested for: (**a**) 2-year survival; (**b**) 3-year survival; (**c**) 5-year survival. The DCA curves can evaluate the clinical benefit of the nomograms and the scope of application. Black indicates that all samples are negative and none are treated, therefore the net benefit is 0. Grey indicates that all samples are positive and all are treated. The x-axis represents threshold probabilities of patients having: (**d**) 2-year survival; (**e**) 3-year survival; (**f**) 5-year survival.

2.9. Comparison of the 11-Gene Risk Model with Other Models

Five prognosis-related risk models were selected, including a 19-gene signature from Yang et al. [23], a 32-gene signature from Willis et al. [24], a 10-gene signature from Wang et al. [25], a 7-gene signature from Sabatier et al. [26] and a 101-gene signature from Millstein et al. [27] to compare with our 11-gene model. To ensure comparability, we calculated a RS of the TCGA-EOC cohort for all five models using the same methods as in our gene signature but based on the corresponding genes of each model. As described, samples were divided into a HRG and a LRG with the median as the threshold. The ROC and KM curves of the five models are shown in Figure 9a–e. Only the AUC of Millstein et al. [27] averaged above our model. No significant difference in prognosis was found among the 7-gene signature, whereas all others confirmed significant differences between the HRG and the LRG.

To compare the predictive performance of these models on EOC, we used the restricted mean survival (RMS) package in R [28] to calculate the C-index of all six models including the 11-gene model. The highest C-index was seen in the 101-gene model, while our C-index ranks second (Figure 9f). We used the RMS time to evaluate the predictive effect of the six models at different time points. The RMS curves showed that the six models had an overlap of 58 months. Under the condition of <58 months, our 11-gene risk model performed better than the models from Yang et al. [23], Willis et al. [24], Wang et al. [25] and Millstein et al. [27] (Figure 9g). Thus, our risk model is more suitable to evaluate the data of <5-year OS.

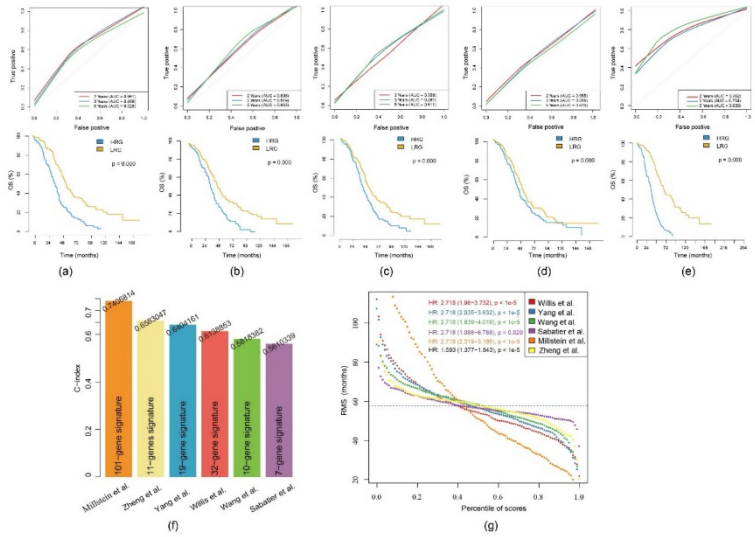

Figure 9. Comparison of the 11-gene risk model with other models: (**a**) The ROC and KM curves of the 19-gene signature (Yang et al.); (**b**) the ROC and KM curves of the 32-gene signature (Willis et al.); (**c**) the ROC and KM curves of the 10-gene signature (Wang et al.); (**d**) the ROC and KM curves of the 7-gene signature (Sabatier et al.); (**e**) the ROC and KM curves of the 101-gene signature (Millstein et al.). (**f**) Concordance indexes (C-indexes) of the six prognostic risk models; (**g**) Restricted mean survival (RMS) time curve of the six prognostic risk models (the dashed line indicates the overlap of 58 months).

2.10. Expression of a Gene Product from the 11-Gene Signature in an EOC Cohort

In a representative EOC cohort from our hospital we measured the expression of the prostaglandin E2 receptor 3 (EP3) encoded by PTGER3, which is upregulated in the HRG compared to the LRG. An immunohistochemistry (IHC) score >1 represents elevated expression of EP3, while an IHC score ≤1 shows low expression. In parallel to the 11-gene signature, higher expression of PTGER3's gene product EP3 is correlated with poor OS in both the whole cohort and the serous subgroup (Figure 10). Even without having found any significance, this finding supports the functionality of the 11-gene signature and could act as a basis for further confirmation of the 11-gene signature in a clinical context.

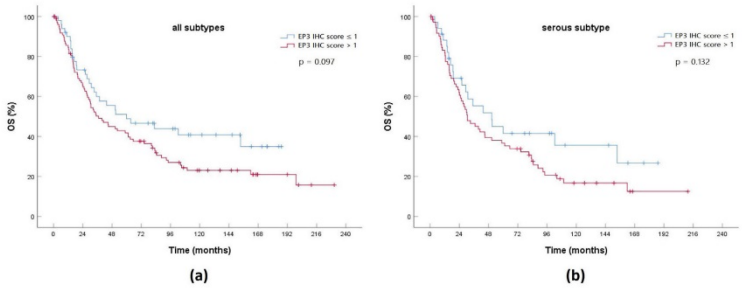

Figure 10. KM curve comparing OS between high prostaglandin E2 receptor 3 (EP3) expression (immunohistochemistry (IHC) score >1) and low EP3 expression (IHC score ≤1) in an EOC cohort for: (**a**) all histological subtypes (n = 151); (**b**) serous subtype (n = 108).

2.11. Translational Level Validation Related to Signature Genes

In order to analyze the translational levels of more signature genes besides PTGER3, the Human Protein Atlas (HPA) database was used. ADORA3, CH25H, CCL19, CXCL9 and CXCL10 were not recorded in the database. The results of PI3, RGS1, CCDC80, PTGER3, MATK and KLRB1 are shown in Figure 11a–f. We found that the expression intensity and quantity of PI3, RGS1, PTGER3 and CCDC80 in ovarian cancer tissue was higher than that in normal ovarian tissue. In contrast, KLRB1's expression intensity and quantity in normal tissue was higher than that in the tumor tissue. Both findings concur with the expression profile in our 11-gene signature. The expression intensity of MATK in ovarian cancer tissue was lower than that in normal tissue, but had a higher expression quantity, which cannot be clearly correlated with the polarity of our signature.

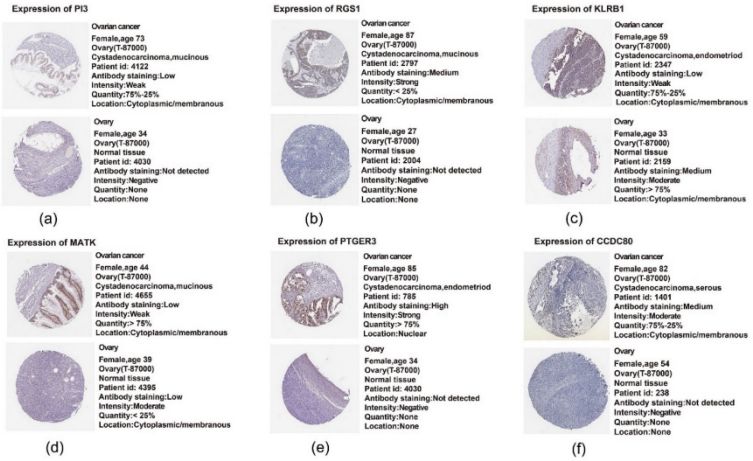

Figure 11. Translational level validation of six genes from the 11-gene signature using the Human Protein Atlas (HPA): (**a**) expression of PI3; (**b**) expression of RGS1; (**c**) expression of KLRB1; (**d**) expression of MATK; (**e**) expression of PTGER3; (**f**) expression of CCDC80.

3. Discussion

Due to the lack of early detection and prevention, 70% of EOC patients present in an advanced stage with distant metastases upon diagnosis, making ovarian carcinoma the leading cause of death among malignant gynecological tumors [1,2,29]. Traditional prognostic criteria are not sufficient in accurately predicting the survival of an individual patient. Multiple large cancer databases, such as TCGA and GEO, offer researchers the opportunity to analyze gene expression data and the corresponding clinical information on a large scale [30,31]. Until now, previous studies on gene expression have seen modifications in the molecular signature between benign and malignant tumors or low and advanced tumor stages [32–34]. Meanwhile, lipidomic analyses of serum samples have confirmed differences in the lipid profile depending on the tumor's dignity [14] and have even been shown to prevent peritoneal metastases when targeting the lipid metabolism signaling axis [15].

Consequently, in this study, 363 EOC samples from the TCGA were subdivided, based on 751 lipid metabolism-related genes, into two subtypes. We report that the prognosis of the C1 subtype is significantly poorer than that of the C2 subtype. This finding suggests that lipid-based molecular subtypes can be used, to a certain extent, as an indication for evaluating the prognosis of patients.

To study the individual role of all the genes of both subtypes, we obtained 925 DEGs, of which 193 were upregulated and 732 were downregulated in the C2 compared to the C1 subtype. These genes were mainly active in the regulation of leukocyte activation, T cell activation, regulation of lymphocyte activation and other immunological functions. The immune cell infiltration scores in C1 were found to be significantly higher than in the C2 subtype. Numerous other studies have pointed out the prognostic significance of tumor-infiltrating lymphocytes in other various cancers [35–38]. It has been reported that tumor infiltration by a subpopulation of CD4+ T cells with immunosuppressive properties predicted reduced survival in EOC [39,40]. Therefore, we can infer that the C1 subtype has a worse prognosis partly because the proportion of CD4+ and CD8+ T cells in the C1 subtype is larger than that in the C2 subtype, as an excessive immune enhancement process might also be a sign of poor prognosis for patients.

Currently, studies on the effect of lipid metabolism on tumor immune functions are being carried out to examine a potential link between both lipids and immune regulation. Interestingly, Wefers et al. [41] discovered that the dysregulation of lipid metabolism in the ascites of EOC patients can affect the immune system by regulating T cell proliferation.

Out of the 925 DEGs, we constructed an 11-gene prognostic risk model based on the genes PI3, RGS1, ADORA3, CH25H, CCDC80, PTGER3, MATK, KLRB1, CCL19, CXCL9 and CXCL10. This model shows a strong robustness and can be used in the prognosis predictions of EOC patients. Calibration plots demonstrated that our nomogram is superior in terms of predictive performance when compared to the grading and FIGO stage. Traditional scores like TNM or FIGO depend on an anatomical spread and, therefore, cannot reflect the biological heterogeneity of EOC [3], which may affect their accuracy.

This is the first prognostic model based on lipid metabolism expression profile. Compared with five other prognostic risk models [23–27] for EOC, the predictive effect of our model at different time points shows that within a survival period of less than 58 months, our 11-gene risk model is the most powerful. Although the model from Millstein et al. [27] has a very high 5-year AUC, it should be noted that their model involves a very large amount of genes, indicating higher costs and consequently reduced clinical utility. Among these 101 genes, the top five genes were TAP1, ZFHX4, CXCL9, FBN1 and PTGER3 ($p < 0.001$), which is interesting because PTGER3 and CXCL9 are in our 11-gene model as well.

While other models did not use the lipid metabolism approach, they also used mainly TCGA data as a base [23–25,27]. Only Sabatier et al. [26] used their own patient cohort. In the 19-gene signature, they initially performed a combination with clinical data, which we did as well in the nomogram [23]. In the model from Wang et al. [25] they already evaluated ten biomarkers from the candidate genes and achieved a 100% accuracy. To optimize an early diagnosis of EOC this access via biomarkers

remains promising and encouraged us to take a more detailed look into some of the 11 genes selected in our model.

PI3 is located on chromosome 20q 12-13.1 [42,43] and encodes elafin, also known as peptidase inhibitor 3. It is reported to be highly expressed in high-grade serous EOC and is associated with a poor prognosis [44,45]. Wei et al. [46] suggested that elafin selectively regulates the sensitivity of EOC cells to genotoxic drug-induced apoptosis. Our results show that the higher the risk value, the higher the expression of PI3 and the poorer the prognosis of EOC patients, which is consistent with the experimental results.

The regulator of G protein signaling 1 is encoded through RGS1, located on chromosome 1q 31.2 [47]. There is increasing evidence for aberrantly differentiated expression of certain members of this protein family in various cancers and their capability of mediating the proliferation or migration of cancer cells [48]. A study had shown that RGS1 is highly expressed in advanced cervical cancer and is associated with cancer progression [49]. So far, besides our identification of RGS1 as a negative prognosticator in this 11-gene model, no other study reported a role of RGS1 in EOC.

Adenosine receptors are a class of purinergic G protein-coupled receptors with adenosine as an endogenous ligand [50], and ADORA3 codes for one of them. In humans, they are involved in the induction of p53-mediated apoptosis. Consequently, in lung cancer cell lines it is used as a target for antibody-based therapy in p53 mutant tumors [51]. In parallel to RGS1, the biological role of ADORA3 in EOC has not been clarified yet but it should be a target for future research due to its high expression in ovarian tissue, as seen in databases.

The gene product of CH25H is cholesterol 25-hydroxylase, which catalyzes the formation of 25-hydroxycholesterol and thereby results in an inhibitive effect on cholesterol biosynthetic enzymes. It is derived and secreted by U87MG and GM133 glioblastoma cell lines and may be involved in the recruitment of immune-competent cells [52,53]. Mittempergher et al. [54] found that CH25H expression is correlated with the prognosis of breast cancer patients and is an independent predictor of distant metastasis, which is consistent with our data.

The prostaglandin receptor EP3, encoded by PTGER3, is one of the four identified receptors that mediate the effects of prostaglandin E2 [55]. In previous work, our IHC assay showed that EP3 is highly expressed in tissues of clear cell ovarian carcinomas and is a prognostic factor in tumor-associated mucin-1 negative EOC [56]. In this model, high expression of EP3 was grouped into the HRG, indicating poor prognosis, which concurs with the previous experimental results. An analysis of the whole patient cohort from Czogalla et al. [56] for both all histologic subtypes and serous subtype also confirmed the correlation between EP3 as a "high-risk" gene and the clinical data. Additionally to EOC, in our lab, EP3 has been identified as an independent risk factor for the survival prognosis of patients with other gynecological malignancies, such as cervical [57], endometrial [58] and breast cancer [59].

In a meta-analysis of the pan-carcinoma resources and expression characteristics of 18,000 human tumors, Gentles et al. [60] found that KLRB1 is the most favorable pan-cancer prognosis gene and is a marker for enhanced innate immune characteristics in different T cell subsets. Consistent with the results of previous studies, we found that the high expression of KLRB1 was located in the LRG with a good prognosis.

However, several limitations in the current research should be considered. Firstly, the TCGA database is mainly constrained to Caucasian and African populations. Therefore, a robust nomogram should be further validated within multicenter clinical trials and prospective studies. Secondly, we do not have experimental data for the majority of these genes to prove the correlation between the 11-gene signature and the prognosis of EOC. Some of these genes have yet to be reported in the context of EOC. Moreover, we need more external independent datasets to further verify our signature even if we proved the robustness of our signature in the GSE32026 verification cohort.

A follow-up study to analyze the translational levels of the proteins belonging to these 11 genes is under work. In clinical environments, this gene signature can primarily be used as an additional tool, as it still must be validated in large patient cohorts. In actuality, the signature might support the shared

decision-making for or against an incriminating therapy in special patient groups, e.g., very old patients or others with relevant comorbidities. Another aspect in regards to personalized treatment could be the patient's RS as an indicator for the adaptation of gyneco-oncological aftercare intervals. Finally, biomarkers or therapeutic drugs resulting from our or other gene signatures mentioned would naturally be the biggest therapeutic gain but need a lot of further research. Nevertheless, in an upcoming era of next generation sequencing and gene expression profiling, which we already use as standard critical diagnostic tests in breast cancer treatment, multiple prognostic gene signatures will grow in relevance in our clinical decision-making.

4. Materials and Methods

4.1. Ovarian Cancer Cohort Source and Preprocessing

The gene expression profiles and clinical follow-up information of EOC were downloaded using the TCGA Genomic Data Commons Application Programming Interface. This cohort contains the expression profile information of 379 RNA-Seq samples of serous EOC. GSE32026 data, downloaded from GEO, covering 260 samples. Human lipid metabolism-related pathways were downloaded from Molecular Signature Database (version 7.0). Herein, a total of 776 lipid metabolism genes (Supplementary Table S7) were sorted out from the six lipid metabolism pathways from the databases KEGG and Reactome (Table 4).

Table 4. Lipid metabolism-related pathways in the Molecular Signature Database.

Pathway	Database	Gene Count
Peroxisome proliferator activated receptor alpha	Reactome	119
Metabolism of lipids	Reactome	738
Sphingolipid metabolism	Reactome	89
Transcriptional regulation of white adipocyte differentiation	Reactome	84
Glycerophospholipid metabolism	KEGG	77
Fatty acid metabolism	Reactome	77
		Total: 1184 Unique: 776

The RNA-Seq data from the TCGA were preprocessed by removing the samples without clinical follow-up information, removing the genes with fragments per kilobase of exon model per million reads mapped less than one and retaining the lipid metabolism gene expression profile. The same procedures were performed on the GSE32026 cohort and the benign tissue samples were removed. A total of 363 samples from the TCGA cohort along with 230 samples from the GSE32026 cohort remained (Table 5).

Table 5. Clinical features of the remaining TCGA and GEO Series 32026 (GSE32026) cohort.

Clinical Feature		TCGA	GSE32026
Event	Censored	141	116
	Dead	222	114
FIGO stage	I	1	
	II	20	
	III	285	
	IV	54	
	None	3	
Age	≤60	191	
	>60	172	
Grade	G1	1	
	G2	42	
	G3	310	
	G4	1	
	None	9	

4.2. Identification of Molecular Subtypes Using NMF Algorithm

We extracted the expression of these 776 lipid metabolism genes from the TCGA expression profile data and retained the samples with a gene expression level above zero; 751 genes remained. Univariable Cox analysis was performed using the coxph function in R package to determine the genes that are correlated with the prognosis expressed as OS of EOC ($p < 0.05$). The NMF was used to cluster the EOC samples under the condition of standard NMF "brunet" for 50 iterations by extracting biological correlation coefficients and internal feature structures of the gene expression matrix. The number of clusters k was identified from 2–10. The average contour width of the common member matrix was determined using the NMF package and the minimum member of each subclass was set to 10. We calculated the optimal number of clusters. The selection was based on the following parameters: cophenetic, residual sum of squares and silhouette.

4.3. Comparison of Molecular Subtype Immune Scores with TIMER

TIMER is a web server for comprehensive analysis of tumor-infiltrating immune cells [61]. The levels of six tumor-infiltrating immune subsets are precalculated for 10,897 tumors from 32 cancer types. It provides six major analytic modules that allow users to interactively explore the associations between immune infiltrates and a wide spectrum of factors, including gene expression, clinical outcome, somatic mutations and somatic copy number alterations.

4.4. Functional Analysis of DEGs

We used the limma package (version 3.42) in R to calculate the DEGs between the different molecular subtypes and filtered these genes in accordance with the threshold of a FDR < 0.05 and |log2(foldchange)| > 1 [62]. Further analysis of the DEGs was performed using clusterProfiler package (version 3.13) [63]. KEGG and GO functional enrichment analysis was conducted. KEGG, a database for the systematic analysis of gene functions, associates genomic information with gene functions and aims to reveal the genetic and chemical blueprint of life. GO enrichment analysis covers three areas including cell components, molecular function, and biological processes.

4.5. Sample Preparation

Firstly, the 363 samples in the TCGA cohort were divided into a training cohort and a validation cohort. In order to prevent the bias of random allocation from undermining the stability of the subsequent modeling, all samples were put back into random groups for 100-times in advance. Herein, the group sampling of the training and validation cohorts was performed in the ratio of 7:3. The most suitable training and validation cohorts were selected according to the following conditions:

- The two cohorts are similar in age distribution, FIGO stage, follow-up time and death rate of patients.
- The gene expression profiles of the two data sets that were randomly grouped were close in the number of classified samples.

Finally, the training set had a total of 253 samples and the validation set had 110 samples in total. The difference between the training set and the validation set was analyzed using a chi-square test.

4.6. Lasso Regression Analysis

We further compressed the genes using lasso regression to reduce the number of genes in the risk model. The lasso method is a compression estimation used to build a more refined model by constructing a penalty function, thereby compressing some coefficients and setting some coefficients to zero [64]. Therefore, it retains the advantage of contraction in subsets. It is a biased estimation that can be used to process complex collinearity data and can realize the simultaneous selection of variables during parameter estimation to optimize the multicollinearity problem in regression analysis. When applying the glmnet

package for lasso Cox regression analysis, we used 3-fold cross validation for model construction and analyzed the CI in each lambda [65].

4.7. Stability Assessment of Risk Model

In order to evaluate the impact of random sampling on the stability of the model, we conducted 1000 instances of random sampling at various proportions in all TCGA samples to evaluate the times of significant difference in the prognosis of the HRG and the LRG samples.

4.8. Construction of Nomogram Combined with RS and Clinical Features

Nomogram is a method to display the results of the risk model intuitively and effectively. It is conveniently applied in the prediction of the outcome. It uses the length of the line to represent the different variables, thereby exhibiting the effect of different variable values on the outcome. We used the TCGA-EOC cohort to build a nomogram that combines FIGO stage, age, grade and RS.

4.9. Analysis of DCA

DCA is a simple method to evaluate clinical predictive models, diagnostic tests and molecular markers. It was initially used as a novel analytical technique that incorporated the clinical consequences of a decision to quantify the clinical utility of a prediction nomogram. Therefore, the DCA can decide whether the predictive nomogram is clinically useful or not. The best model is one with a high net benefit as calculated within the favorable probability.

4.10. IHC of EP3 in an EOC Patient Cohort

The specimens derived from a cohort consisting of 151 patients with epithelial EOC (serous: n = 108, endometrioid: n = 20, clear cell: n = 11, mucinous n = 12) who underwent radical cytoreductive surgery in our department between 1990 and 2002. Diagnoses were done by a specialized gynecologic pathologist. Advanced disease (FIGO IIB-IV) presented in approximately three quarters of the specimens. Mean age at primary diagnosis was 58.9 years. All patients, except FIGO stage IA, received adjuvant platinum-based chemotherapy. Lifetime data were taken from our patient charts, the Munich Cancer Registry and aftercare calendars. The study was carried out in compliance with the guidelines of the Helsinki Declaration of 1964 (last revision October 2018). All participants gave their written informed consent.

The procedure of IHC has been previously described in our lab [57–59]. We stained tissue microarrays of the EOC samples of paraffin-embedded and formalin-fixed tissues after epitope retrieval with primary polyclonal anti-EP3 rabbit IgG (Abcam, Cambridge, UK). Afterwards, detection was performed via polymer method with ZytoChem Plus HRP Polymer System mouse/ rabbit (Zytomed Systems, Berlin, Germany) and the chromogen diaminobenzidine (Dako, Hamburg, Germany).

The IHC staining was assessed semiquantitatively, according to Remmele and Stegner [66], using the IHC score. EP3 expression was regarded as negative with an IHC score 0–1 and as positive with an IHC score >1. Expression-dependent differences in OS were tested by chi-square statistic of the Log-Rank test (Mantel-Cox) in KM curves with SPSS Statistics 25 (IBM, Chicago, IL, USA).

4.11. Translational Level Validation of Signature Genes

The HPA was initiated in 2003 and shows the expression and localization of human proteins across tissues and organs. It is based on deep RNA-seq from 37 major tissue types and IHC on tissue microarrays containing 44 different tissue types. Altogether, 76 different cell types, covering all major parts of the human body, have been analyzed manually and the data are presented as histology-based annotation of protein expression levels. The antibody-based protein profiles are qualitative and describe the spatial distribution, cell type specificity and the rough relative abundance of proteins in these tissues, whereas the mRNA data provide quantitative data on the average gene expression within an entire

tissue. For each gene, the immunohistochemical staining profile is matched with mRNA data and gene/protein characterization data to yield an "annotated protein expression" profile.

5. Conclusions

In conclusion, we propose the first 11-gene signature (PI3, RGS1, ADORA3, CH25H, CCDC80, PTGER3, MATK, KLRB1, CCL19, CXCL9 and CXCL10) prediction model based on lipid metabolism-related genes in EOC. Despite different drawbacks of the current analysis, this model may be an interesting approach for a molecular diagnostic test assessing the prognosis and possible risk factors of EOC patients. Furthermore, the development of biomarkers based on this gene signature could represent a perspective for the clinical care of cancer patients.

Supplementary Materials: The following are available online at http://www.mdpi.com/1422-0067/21/23/9169/s1.

Author Contributions: Conceptualization, M.Z., U.J., F.T., S.M. and T.K.; data curation, M.Z.; formal analysis, M.Z. and T.K.; investigation, M.Z., A.H., B.C., H.H., T.V., A.V., A.C.-R. and T.K.; methodology, M.Z. and T.K.; project administration, U.J., F.T., S.M. and T.K.; resources, M.Z., B.C., H.H., T.V., A.V., A.C.-R. and T.K.; software, M.Z. and A.H.; supervision, U.J., F.T., S.M. and T.K.; validation, M.Z., U.J. and T.K.; visualization, M.Z. and T.K.; writing—original draft, M.Z.; writing—review and editing, H.M. and T.K. All authors have read and agreed to the published version of the manuscript.

Funding: We acknowledge financial support by the China Scholarship Council for Mingjun Zheng and by the Friedrich-Baur-Stiftung (registration number 33/19) for Till Kaltofen.

Acknowledgments: The results shown here are in whole or part based upon data generated by TCGA (https://www.cancer.gov/tcga), KEGG (https://www.genome.jp/kegg), GO (http://geneontology.org), GEO (https://www.ncbi.nlm.nih.gov/geo), Reactome (https://reactome.org), Molecular Signature Database (https://www.gsea-msigdb.org/gsea/msigdb/index.jsp) and HPA (http://www.proteinatlas.org).

Conflicts of Interest: F.T.: Research support, advisory board, honoraria and travel expenses from AstraZeneca, Clovis, Medac, PharmaMar, Roche and Tesaro. S.M.: Research support, advisory board, honoraria and travel expenses from AbbVie, AstraZeneca, Clovis, Eisai, GlaxoSmithKline, Medac, MSD, Novartis, Olympus, PharmaMar, Pfizer, Roche, Sensor Kinesis, Teva and Tesaro. The funders had no role in the design of the study; in the collection, analyses, or interpretation of data; in the writing of the manuscript, or in the decision to publish the results. The other authors declare no conflict of interest.

Abbreviations

AUC	area under the curve
C1	cluster 1
C2	cluster 2
C-index	concordance index
CI	confidence interval
DCA	decision curve analysis
DEG	differentially expressed gene
EOC	epithelial ovarian cancer
FDR	false discovery rate
FIGO	Fédération Internationale de Gynécologie et d'Obstétrique
GEO	Gene Expression Omnibus
GO	Gene Ontology
GSE32026	GEO Series 32026
HPA	Human Protein Atlas
HR	hazard ratio
HRG	high-risk group
IHC	immunohistochemistry
KEGG	Kyoto Encyclopedia of Genes and Genomes
KM	Kaplan-Meier
LRG	low-risk group
NMF	non-negative matrix factorization
OS	overall survival
EP3	prostaglandin E2 receptor 3
RMS	restricted mean survival
ROC	receiver operating characteristic
RS	risk score
TCGA	The Cancer Genome Atlas
TIMER	Tumor Immune Estimation Resource

References

1. Siegel, R.L.; Miller, K.D.; Jemal, A. Cancer statistics 2019. *CA Cancer J. Clin.* **2019**, *69*, 7–34. [PubMed]
2. Waldmann, A.; Eisemann, N.; Katalinic, A. Epidemiology of malignant cervical, corpus uteri and ovarian tumours-current data and epidemiological trends. *Geburtshilfe Frauenheilkd* **2013**, *73*, 123–129. [PubMed]
3. Jayson, G.C.; Kohn, E.C.; Kitchener, H.C.; Ledermann, J.A. Ovarian cancer. *Lancet* **2014**, *384*, 1376–1388. [PubMed]
4. Howlader, N.; Noone, A.M.; Krapcho, M.; Miller, D.; Brest, A.; Yu, M.; Ruhl, J.; Tatalovich, Z.; Mariotto, A.; Lewis, D.R.; et al. (Eds.) *SEER Cancer Statistics Review, 1975–2016*; based on November 2018 SEER data submission; National Cancer Institute: Bethesda, MD, USA, 2019.
5. Lech, A.; Daneva, T.; Pashova, S.; Gagov, H.; Crayton, R.; Kukwa, W.; Czarnecka, A.M.; Szczylik, C. Ovarian cancer as a genetic disease. *Front. Biosci.* **2013**, *18*, 543–563.
6. Eng, K.H.; Weir, I.; Tsuji, T.; Odunsi, K. Immuno-stimultory/regulatory gene expression patterns in advanced ovarian cancer. *Genes Cancer* **2015**, *6*, 399–407.
7. Mittempergher, L. Genomic characterization of high-grade serous ovarian cancer: Dissecting its molecular heterogeneity as a road towards effective therapeutic strategies. *Curr. Oncol. Rep.* **2016**, *18*, 44.
8. Cai, S.Y.; Yang, T.; Chen, Y.; Wang, J.W.; Li, L.; Xu, M.J. Gene expression profiling of ovarian carcinomas and prognostic analysis of outcome. *J. Ovarian Res.* **2015**, *8*, 50.
9. Tassi, R.A.; Todeschini, P.; Siegel, E.R.; Calza, S.; Cappella, P.; Ardighieri, L.; Cadei, M.; Bugatti, M.; Romani, C.; Bandiera, E.; et al. FOXM1 expression is significantly associated with chemotherapy resistance and adverse prognosis in non-serous epithelial ovarian cancer patients. *J. Exp. Clin. Cancer Res.* **2017**, *36*, 63.
10. Niemi, R.J.; Braicu, E.I.; Kulbe, H.; Koistinen, K.M.; Sehouli, J.; Puistola, U.; Mäenpää, U.J.; Hilvo, M. Ovarian tumours of different histologic type and clinical stage induce similar changes in lipid metabolism. *Br. J. Cancer* **2018**, *119*, 847–854.
11. Nickels, J.T. New links between lipid accumulation and cancer progression. *J. Biol. Chem.* **2018**, *293*, 6635–6636.
12. Xu, Y. Lysophospholipid signaling in the epithelial ovarian cancer tumor microenvironment. *Cancers* **2018**, *10*, 227.
13. Zhao, G.; Cardenas, H.; Matei, D. Ovarian cancer-why lipids matter. *Cancers* **2019**, *10*, 1870.
14. Braicu, E.I.; Darb-Esfahani, S.; Schmitt, W.D.; Koistinen, K.M.; Heiskanen, L.; Pöhö, P.; Budczies, J.; Kuhberg, M.; Dietel, M.; Frezza, C.; et al. High-grade ovarian serous carcinoma patients exhibit profound alterations in lipid metabolism. *Oncotarget* **2017**, *8*, 102912–102922. [PubMed]
15. Chen, R.R.; Yung, M.M.; Xuan, Y.; Zhan, S.; Leung, L.L.; Liang, R.R.; Leung, T.H.Y.; Yang, H.; Xu, D.; Sharma, R.; et al. Targeting of lipid metabolism with a metabolic inhibitor cocktail eradicates peritoneal metastases in ovarian cancer cells. *Commun. Biol.* **2019**, *2*, 281.
16. Cui, T.; Zhang, L.; Huang, Y.; Yi, Y.; Tan, P.; Zhao, Y.; Hu, Y.; Xu, L.; Li, E.; Wang, D. MNDR v2.0: An updated resource of ncRNA–disease associations in mammals. *Nucleic Acids Res.* **2017**, *46*, D371–D374.
17. Liang, Z.Y.; Lai, H.Y.; Yang, H.; Zhang, C.J.; Yang, H.; Wei, H.H.; Chen, X.X.; Zhao, Y.W.; Su, Z.D.; Li, W.C.; et al. Pro54DB: A database for experimentally verified sigma-54 promoters. *Bioinformatics* **2017**, *33*, 467–469.
18. Hu, B.; Zheng, L.; Long, C.; Song, M.; Li, T.; Yang, L.; Zuo, Y. EmExplorer: A database for exploring time activation of gene expression in mammalian embryos. *Open Biol.* **2019**, *9*, 190054.
19. Wang, Z.; Gerstein, M.; Snyder, M. RNA-Seq: A revolutionary tool for transcriptomics. *Nat. Rev. Genet.* **2009**, *10*, 57–63.
20. Yang, H.; Lv, H.; Ding, H.; Chen, W.; Lin, H. iRNA-2OM: A sequence-based predictor for identifying 2′-O-methylation sites in homo sapiens. *J. Comput. Biol.* **2018**, *25*, 1266–1277.
21. Safonov, A.; Jiang, T.; Bianchini, G.; Győrffy, B.; Karn, T.; Hatzis, C.; Pusztai, L. Immune gene expression is associated with genomic aberrations in breast cancer. *Cancer Res.* **2017**, *77*, 3317–3324.
22. Yang, L.; Wang, S.; Zhang, Q.; Pan, Y.; Lv, Y.; Chen, X.; Zuo, Y.; Hao, D. Clinical significance of the immune microenvironment in ovarian cancer patients. *Mol. Omics* **2018**, *14*, 341–351. [CrossRef] [PubMed]
23. Yang, R.; Xiong, J.; Deng, D.; Wang, Y.; Liu, H.; Jiang, G.; Peng, Y.; Peng, X.; Zeng, X. An integrated model of clinical information and gene expression for prediction of survival in ovarian cancer patients. *Transl. Res.* **2016**, *172*, 84–95. [CrossRef] [PubMed]
24. Willis, S.; Villalobos, V.M.; Gevaert, O.; Abramovitz, M.; Williams, C.; Sikic, B.I.; Leyland-Jones, B. Single gene prognostic biomarkers in ovarian cancer: A meta-analysis. *PLoS ONE* **2016**, *11*, e0149183. [CrossRef] [PubMed]

25. Wang, L.; Wang, L.; Ma, L.; Liu, J.; Ma, S. Identifying gene signature for the detection of ovarian cancer based on the achieved related genes. *Gynecol. Obstet. Investig.* **2017**, *82*, 361–370. [CrossRef] [PubMed]
26. Sabatier, R.; Finetti, P.; Bonensea, J.; Jacquemier, J.; Adelaide, J.; Lambaudie, E.; Viens, P.; Birnbaum, D.; Bertucci, F. A seven-gene prognostic model for platinum-treated ovarian carcinomas. *Br. J. Cancer* **2011**, *105*, 304–311. [CrossRef] [PubMed]
27. Millstein, J.; Budden, T.; Goode, E.L.; Anglesio, M.S.; Talhouk, A.; Intermaggio, M.P.; Leong, H.S.; Chen, S.; Elatre, W.; Gilks, B.; et al. Prognostic gene expression signature for high-grade serous ovarian cancer. *Ann. Oncol.* **2020**, *31*, 1240–1250. [CrossRef]
28. Royston, P.; Parmar, M.K.B. Restricted mean survival time: An alternative to the hazard ratio for the design and analysis of randomized trials with a time-to-event outcome. *BMC Med. Res. Methodol.* **2013**, *13*, 152. [CrossRef]
29. Herzog, T.J. Recurrent ovarian cancer: How important is it to treat to disease progression? *Clin. Cancer Res.* **2004**, *10*, 7439–7449. [CrossRef]
30. Nagasawa, S.; Ikeda, K.; Horie-Inoue, K.; Sato, S.; Itakura, A.; Takeda, S.; Hasegawa, K.; Inoue, S. Systematic identification of characteristic genes of ovarian clear cell carcinoma compared with high-grade serous carcinoma based on RNA-sequencing. *Int. J. Mol. Sci.* **2019**, *20*, 4330. [CrossRef]
31. Seborova, K.; Vaclavikova, R.; Soucek, P.; Elsnerova, K.; Bartakova, A.; Cernaj, P.; Bouda, J.; Rob, L.; Hruda, M.; Dvorak, P. Association of ABC gene profiles with time to progression and resistance in ovarian cancer revealed by bioinformatics analyses. *Cancer Med.* **2019**, *8*, 606–616. [CrossRef]
32. Zhang, Z.; Huang, K.; Gu, C.; Zhao, L.; Wang, N.; Wang, X.; Zhao, D.; Zhang, C.; Lu, Y.; Meng, Y. Molecular subtyping of serous ovarian cancer based on multi-omics data. *Sci. Rep.* **2016**, *6*, 26001. [CrossRef] [PubMed]
33. Tothill, R.W.; Tinker, A.V.; George, J.; Brown, R.; Fox, S.B.; Lade, S.; Johnson, D.S.; Trivett, M.K.; Etemadmoghadam, D.; Locandro, B.; et al. Novel molecular subtypes of serous and endometrioid ovarian cancer linked to clinical outcome. *Clin. Cancer Res.* **2008**, *14*, 5198–5208. [CrossRef] [PubMed]
34. Zhang, D.; Chen, P.; Zheng, C.H.; Xia, J. Identification of ovarian cancer subtype-specific network modules and candidate drivers through an integrative genomics approach. *Oncotarget* **2016**, *7*, 4298–4309. [CrossRef] [PubMed]
35. Clemente, G.C.; Mihm, C.M.; Zurrida, S.; Collini, P.; Cascineelli, N. Prognostic value of tumor infiltrating lymphocytes in the vertical growth phase of primary cutaneous melanoma. *Cancer* **1996**, *77*, 1303–1310. [CrossRef]
36. Rozek, L.S.; Schmit, S.L.; Greenson, J.K.; Tomsho, L.P.; Rennert, H.S.; Rennert, G.; Gruber, S.B. Tumor-infiltrating lymphocytes, crohn's-like lymphoid reaction, and survival from colorectal cancer. *J. Natl. Cancer Inst.* **2016**, *108*, djw027. [CrossRef] [PubMed]
37. Naito, Y.; Saito, K.; Shiiba, K.; Ohuchi, A.; Saigenji, K.; Nagura, H.; Ohtani, H. CD8+ T cells infiltrated within cancer cell nests as a prognostic factor in human colorectal cancer. *Cancer Res.* **1998**, *58*, 3491–3494.
38. Nakano, O.; Sato, M.; Naito, Y.; Suzuki, K.; Orikasa, S.; Aizawa, M.; Suzuki, Y.; Shintaku, I.; Nagura, H.; Ohtani, H. Proliferative activity of intratumoral CD8(+) T-lymphocytes as a prognostic factor in human renal cell carcinoma: Clinicopathologic demonstration of antitumor immunity. *Cancer Res* **2001**, *61*, 5132–5136.
39. Sato, E.; Olson, S.H.; Ahn, J.; Bundy, B.; Nishikawa, H.; Qian, F.; Junbluth, A.A.; Frosina, D.; Gnjatic, S.; Ambrosone, C.; et al. Intraepithelial CD8+ tumor-infiltrating lymphocytes and a high CD8+/regulatory T cell ratio are associated with favorable prognosis in ovarian cancer. *Proc. Natl. Acad. Sci. USA* **2005**, *102*, 18538–18543. [CrossRef]
40. Diederichsen, A.C.; Hjelmborg, J.V.B.; Christensen, P.B.; Zeuthen, J.; Fenger, C. Prognostic value of the CD4+/CD8+ ratio of tumour infiltrating lymphocytes in colorectal cancer and HLA-DR expression on tumour cells. *Cancer Immunol. Immunother.* **2003**, *52*, 423–428. [CrossRef]
41. Wefers, C.; Duiveman-de Boer, T.; Zusterzeel, P.L.M.; Massuger, L.F.A.G.; Fuchs, D.; Torensma, R.; Wheelock, C.E.; de Vries, I.J.M. Different lipid regulation in ovarian cancer: Inhibition of the immune system. *Int. J. Mol. Sci.* **2018**, *19*, 273. [CrossRef]
42. Schalkwijk, J.; Wiedow, O.; Hirose, S. The trappin gene family: Proteins defined by an N-terminal transglutaminase substrate domain and a C-terminal four-disulphide core. *Biochem. J.* **1999**, *340*, 569–577. [CrossRef] [PubMed]
43. Clauss, A.; Lilja, H.; Lundwall, Å. A locus on human chromosome 20 contains several genes expressing protease inhibitor domains with homology to whey acidic protein. *Biochem. J.* **2002**, *368*, 233–242. [CrossRef] [PubMed]

44. Labidi-Galy, S.I.; Clauss, A.; Ng, V.; Duraisamy, S.; Elias, K.M.; Piao, H.Y.; Bilal, E.; Davidowitz, R.A.; Lu, Y.; Badalian-Very, G.; et al. Elafin drives poor outcome in high-grade serous ovarian cancers and basal-like breast tumors. *Oncogene* **2015**, *34*, 373–383. [CrossRef] [PubMed]
45. Clauss, A.; Ng, V.; Liu, J.; Piao, H.; Russo, M.; Vena, N.; Sheng, Q.; Hirsch, M.S.; Bonome, T.; Matulonis, U.; et al. Overexpression of elafin in ovarian carcinoma is driven by genomic gains and activation of the nuclear factor κB pathway and is associated with poor overall survival. *Neoplasia* **2010**, *12*, 161–172. [CrossRef]
46. Wei, H.; Hellström, K.E.; Hellström, I. Elafin selectively regulates the sensitivity of ovarian cancer cells to genotoxic drug-induced apoptosis. *Gynecol. Oncol.* **2012**, *125*, 727–733. [CrossRef]
47. Bou, D.J.; Lee, J.K. Regulator of G-Protein signaling 1 (RGS1). In *Encyclopedia of Signaling Molecules*, 2nd ed.; Choi, S., Ed.; Springer International Publishing: Basel, Switzerland, 2018.
48. Sethakorn, N.; Dulin, N.O. RGS expression in cancer: Oncomining the cancer microarray data. *J. Recept. Signal. Transduct. Res.* **2013**, *33*, 166–171. [CrossRef]
49. Wong, Y.F.; Cheung, T.H.; Tsao, G.S.; Lo, K.W.; Yim, S.F.; Wang, V.W.; Heung, M.M.; Chan, S.C.; Chan, L.K.; Ho, T.W.; et al. Genome-wide gene expression profiling of cervical cancer in Hong Kong women by oligonucleotide microarray. *Int. J. Cancer* **2006**, *118*, 2461–2469. [CrossRef]
50. Fredholm, B.B.; IJzerman, A.P.I.; Jacobson, K.A.; Klotz, K.N.; Linden, J. International Union of Pharmacology–XXV. Nomenclature and classification of adenosine receptors. *Pharmacol. Rev.* **2001**, *53*, 527–552.
51. Riccardo, F.; Arigoni, M.; Buson, G.; Zago, E.; Iezzi, M.; Longo, D.; Carrara, M.; Fiore, A.; Nuzzo, S.; Bicciato, S.; et al. Characterization of a genetic mouse model of lung cancer: A promise to identify non-small cell lung cancer therapeutic targets and biomarkers. *BMC Genom.* **2014**, *15*, S1. [CrossRef]
52. Doms, A.; Sanabria, T.; Hansen, J.N.; Altan-Bonnet, N.; Holm, G.H. 25-Hydroxycholesterol production by the cholesterol-25-Hydroxylase interferon-stimulated gene restricts mammalian Reovirus infection. *J. Virol.* **2018**, *92*, e01047-18. [CrossRef]
53. Bauman, D.R.; Bitmansour, A.D.; McDonald, J.G.; Thompson, B.M.; Liang, G.; Russell, D.W. 25-Hydroxycholesterol secreted by macrophages in response to toll-like receptor activation suppresses immunoglobulin A production. *Proc. Natl. Acad. Sci. USA* **2009**, *106*, 16764–16769. [CrossRef] [PubMed]
54. Mittempergher, L.; Saghatchian, M.; Wolf, D.M.; Michiels, S.; Canisius, S.; Dessen, P.; Delaloge, S.; Lazar, V.; Benz, S.C.; Tursz, T.; et al. A gene signature for late distant metastasis in breast cancer identifies a potential mechanism of late recurrences. *Mol. Oncol.* **2013**, *7*, 987–999. [CrossRef] [PubMed]
55. Sugimoto, Y.; Narumiya, S. Prostaglandin E receptors. *J. Biol. Chem.* **2007**, *282*, 11613–11617. [CrossRef] [PubMed]
56. Czogalla, B.; Kuhn, C.; Heublein, S.; Schmöckel, E.; Mayr, D.; Kolben, T.; Trillsch, F.; Burges, A.; Mahner, S.; Jeschke, U.; et al. EP3 receptor is a prognostic factor in TA-MUC1-negative ovarian cancer. *J. Cancer Res. Clin. Oncol.* **2019**, *145*, 2519–2527. [CrossRef] [PubMed]
57. Heidegger, H.; Dietlmeier, S.; Ye, Y.; Kuhn, C.; Vattai, A.; Aberl, C.; Jeschke, U.; Mahner, S.; Kost, B. The prostaglandin EP3 receptor is an independent negative prognostic factor for cervical cancer patients. *Int. J. Mol. Sci.* **2017**, *18*, 1571. [CrossRef]
58. Zhu, J.; Trillsch, F.; Mayr, D.; Kuhn, C.; Rahmeh, M.; Hofmann, S.; Vogel, M.; Mahner, S.; Jeschke, U.; Schönfeldt, V. Prostaglandin receptor EP3 regulates cell proliferation and migration with impact on survival of endometrial cancer patients. *Oncotarget* **2018**, *9*, 982–994. [CrossRef]
59. Semmlinger, A.; von Schoenfeldt, V.; Wolf, V.; Meuter, A.; Kolben, T.M.; Kolben, T.; Zeder-Goess, C.; Weis, F.; Gallwas, J.; Wuerstlein, R.; et al. EP3 (prostaglandin E2 receptor 3) expression is a prognostic factor for progression-free and overall survival in sporadic breast cancer. *BMC Cancer* **2018**, *18*, 431. [CrossRef]
60. Gentles, A.J.; Newman, A.M.; Liu, C.L.; Bratman, S.V.; Feng, W.; Kim, D.; Nair, V.S.; Xu, Y.; Khuong, A.; Hoang, C.D.; et al. The prognostic landscape of genes and infiltrating immune cells across human cancers. *Nat. Med.* **2015**, *21*, 938–945. [CrossRef]
61. Li, T.; Fan, J.; Wang, B.; Traugh, N.; Chen, Q.; Liu, J.S.; Li, B.; Liu, X.S. TIMER: A web server for comprehensive analysis of tumor-infiltrating immune cells. *Cancer Res.* **2017**, *77*, e108–e110. [CrossRef]
62. Ritchie, M.E.; Phipson, B.; Wu, D.; Hu, Y.; Law, C.W.; Shi, W.; Smyth, G.K. Limma powers differential expression analyses for RNA-sequencing and microarray studies. *Nucleic Acids Res.* **2015**, *43*, e47. [CrossRef]
63. Yu, G.; Wang, L.G.; Han, Y.; He, Q.Y. ClusterProfiler: An R package for comparing biological themes among gene clusters. *Omics* **2012**, *16*, 284–287. [CrossRef] [PubMed]
64. Tibshirani, R. Regression shrinkage and selection via the lasso. *J. R. Stat. Soc. B* **1996**, *58*, 267–288. [CrossRef]

65. Friedman, J.; Hastie, T.; Tibshirani, R. Regularization paths for generalized linear models via coordinate descent. *J. Stat. Softw.* **2010**, *33*, 1–22. [CrossRef] [PubMed]
66. Remmele, W.; Stegner, H.E. Recommendation for uniform definition of an immunoreactive score (IRS) for immunohistochemical estrogen receptor detection (ER-ICA) in breast cancer tissue. *Pathologe* **1987**, *8*, 138–140. [PubMed]

6. Paper II

Zheng M, Long J, Chelariu-Raicu A, Mullikin H, Vilsmaier T, Vattai A, Heidegger HH, Batz F, Keckstein S, Jeschke U, Trillsch F, Mahner S, Kaltofen T. **Identification of a Novel Tumor Microenvironment Prognostic Signature for Advanced-Stage Serous Ovarian Cancer**. *Cancers*. 2021; 13(13):3343. https://doi.org/10.3390/cancers13133343

cancers

MDPI

Article

Identification of a Novel Tumor Microenvironment Prognostic Signature for Advanced-Stage Serous Ovarian Cancer

Mingjun Zheng [1,†], Junyu Long [2,†], Anca Chelariu-Raicu [1], Heather Mullikin [1,3], Theresa Vilsmaier [1], Aurelia Vattai [1], Helene Hildegard Heidegger [1], Falk Batz [1], Simon Keckstein [1], Udo Jeschke [1,4,*], Fabian Trillsch [1], Sven Mahner [1] and Till Kaltofen [1,*]

[1] Department of Obstetrics and Gynecology, University Hospital, LMU Munich, Marchioninistrasse 15, 81377 Munich, Germany; Mingjun.Zheng@med.uni-muenchen.de (M.Z.); Anca.ChelariuRaicu@med.uni-muenchen.de (A.C.-R.); Heather.Mullikin@ukr.de (H.M.); Theresa.Vilsmaier@med.uni-muenchen.de (T.V.); Aurelia.Vattai@med.uni-muenchen.de (A.V.); Helene.Heidegger@med.uni-muenchen.de (H.H.H.); Falk.Batz@med.uni-muenchen.de (F.B.); Simon.Keckstein@med.uni-muenchen.de (S.K.); Fabian.Trillsch@med.uni-muenchen.de (F.T.); Sven.Mahner@med.uni-muenchen.de (S.M.)

[2] Department of Liver Surgery, Peking Union Medical College Hospital, Chinese Academy of Medical Sciences & Peking Union Medical College, 9 Dongdan 3rd Alley, Dongcheng District, Beijing 100730, China; Lancet_Junyu@163.com

[3] Department of Gynecology and Obstetrics, University Medical Center Regensburg, Landshuter Strasse 65, 93053 Regensburg, Germany

[4] Department of Obstetrics and Gynecology, University Hospital Augsburg, Stenglinstrasse 2, 86156 Augsburg, Germany

* Correspondence: Udo.Jeschke@med.uni-muenchen.de (U.J.); Till.Kaltofen@med.uni-muenchen.de (T.K.); Tel.: +49-89-440054111 (U.J. & T.K.)

† Mingjun Zheng and Junyu Long contributed equally to this paper.

check for updates

Citation: Zheng, M.; Long, J.; Chelariu-Raicu, A.; Mullikin, H.; Vilsmaier, T.; Vattai, A.; Heidegger, H.H.; Batz, F.; Keckstein, S.; Jeschke, U.; et al. Identification of a Novel Tumor Microenvironment Prognostic Signature for Advanced-Stage Serous Ovarian Cancer. *Cancers* **2021**, *13*, 3343. https://doi.org/10.3390/cancers13133343

Academic Editor: Mary Frances McMullin

Received: 31 May 2021
Accepted: 29 June 2021
Published: 3 July 2021

Publisher's Note: MDPI stays neutral with regard to jurisdictional claims in published maps and institutional affiliations.

Simple Summary: The expression of tumor microenvironment-related genes is known to be correlated with ovarian cancer patients' prognosis. Immunotherapeutic targets are in part located in this complex cluster of cells and soluble factors. In our study, we constructed a prognostic 11-gene signature for advanced serous ovarian cancer from tumor microenvironment-related genes through lasso regression. The established risk score can quantify the prognosis of ovarian cancer patients more accurately and is able to predict the putative biological response of cancer samples to a programmed death ligand 1 blocking immunotherapy. This might empower the role of immunotherapy in ovarian cancer through its usage in future study protocols.

Abstract: (1) Background: The tumor microenvironment is involved in the growth and proliferation of malignant tumors and in the process of resistance towards systemic and targeted therapies. A correlation between the gene expression profile of the tumor microenvironment and the prognosis of ovarian cancer patients is already known. (2) Methods: Based on data from The Cancer Genome Atlas (379 RNA sequencing samples), we constructed a prognostic 11-gene signature (*SNRPA1*, *CCL19*, *CXCL11*, *CDC5L*, *APCDD1*, *LPAR2*, *PI3*, *PLEKHF1*, *CCDC80*, *CPXM1* and *CTAG2*) for Fédération Internationale de Gynécologie et d'Obstétrique stage III and IV serous ovarian cancer through lasso regression. (3) Results: The established risk score was able to predict the 1-, 3- and 5-year prognoses more accurately than previously known models. (4) Conclusions: We were able to confirm the predictive power of this model when we applied it to cervical and urothelial cancer, supporting its pan-cancer usability. We found that immune checkpoint genes correlate negatively with a higher risk score. Based on this information, we used our risk score to predict the biological response of cancer samples to an anti-programmed death ligand 1 immunotherapy, which could be useful for future clinical studies on immunotherapy in ovarian cancer.

Keywords: ovarian neoplasms; tumor microenvironment; genes; The Cancer Genome Atlas (TCGA); immunotherapy

1. Introduction

Ovarian cancer (OC) has the highest mortality rate among malignancies originating in the female reproductive system. Given the continuous improvement of both diagnostic techniques and treatment methods, the prevalence and survival rate of OC patients have increased during the past 15 years. More specifically, the prevalence of OC was recently reported to be 10 times higher than its incidence [1]. OC accounts for 3.3% of all malignant diseases in women in Germany and the cancer-related mortality rate is high, accounting for 5.6% of all malignancy-related deaths [2]. Advanced-stage serous ovarian cancer (SOC) is the cause of most OC deaths. Although 80% of patients significantly benefit from surgery and chemotherapy, they usually relapse and metastasize and are, therefore, incurable. Approximately two-thirds will experience a relapse after receiving several lines of therapy and die within 10 years of the first diagnosis [3,4].

At present, Fédération Internationale de Gynécologie et d'Obstétrique (FIGO), TNM stage and *BRCA1/2* status are the most relevant clinical variables to guide the management of SOC patients [5]. However, due to the high heterogeneity of SOC, which is the most important and representative entity, among others, the prognosis of patients with similar clinical characteristics can be very different. In addition, the analysis of messenger RNA expression, microRNA expression, promoter methylation and DNA copy number in 489 high-grade SOCs from The Cancer Genome Atlas (TCGA) indicated different molecular signatures in tumors with serous histology. Moreover, a defective homologous recombination is critical for choosing a maintenance therapy in the first-line situation at present [6]. Therefore, by using gene signatures as biomarkers, personalized therapy can be optimized and, subsequently, the clinical outcome of advanced-stage SOC patients could be improved.

The tumor microenvironment (TME) consists of a complex system of immune, inflammation and myeloid-derived suppressor cells as well as fibroblasts, macrophages, vasculature and various soluble factors [7,8]. Generally, this dynamic biological system sustains the development of malignant tumors and plays a crucial regulatory role in the emergence of resistance to chemotherapy and targeted therapy [9,10]. Previous studies have shown that upregulated expression of TME genes might correlate with the clinical outcome of OC patients. In particular, increased levels of the serum-soluble tumor necrosis factor receptor 2 may indicate a poor prognosis, as it was significantly higher in samples collected from malignant tumors compared to samples from benign neoplasms [11]. Furthermore, the presence of tumor-associated macrophages was associated with tumor progression, including cell invasion, metastasis, angiogenesis and early recurrence [8,12,13]. In contrast, another analysis of 1731 tumors obtained from SOC patients indicated that high levels of activated dendritic tumor-infiltrating lymphocytes were associated with a good prognosis [14,15].

Taken together, these results indicate that exploring the TME has an important role in assessing the prognosis of OC patients and angiogenesis or immune checkpoint inhibitors, which are currently in phase II/III clinical trials, and represent targeted therapies to TME components [16–18]. Considering that the TME in OC tumors is highly heterogeneous [19], a TME-related gene signature might improve the accuracy of predicting clinical response to targeted therapy. Consequently, with this study, we are aiming to design a gene signature based on TME-related genes and, further, we will attempt to use the developed signature to predict the response to immune checkpoint inhibitors.

2. Materials and Methods

2.1. Data Download and Preprocessing

The Genomic Data Commons Application Programming Interface portal was used to download the gene expression profiles from SOC patients. The data based on TCGA and the cohort contained 379 RNA sequencing samples. We processed the RNA sequencing data of TCGA by removing the samples without clinical follow-up information and retaining the expression profile of TME-related genes only for FIGO stage III and IV samples. Finally, 347 SOC samples were included.

Moreover, for external validation, the Australian OC cohort from the International Cancer Genome Consortium (ICGC) was downloaded. Samples without clinical follow-up information were removed and only FIGO stage III and IV samples were retained. After this process, 93 samples from the ICGC cohort remained.

TME-related genes were obtained from published research [20–26], which, after sorting, provided 4061 genes (Table S1).

2.2. Identification of Molecular Subtypes Using Non-Negative Matrix Factorization (NMF) Algorithm

The expression levels of the 4061 TME genes were extracted from TCGA expression profile and a univariable Cox analysis was performed using the coxph function [27,28] to obtain prognostic genes of OC ($p < 0.01$). NMF was used to cluster the samples for 50 iterations by extracting biological correlation coefficients and internal feature structures of the prognostic gene expression matrix [29]. The number of clusters k was from 2–10. When k = 3, the cluster demonstrated proper stability and performance, resulting in the clusters 1, 2 and 3 (C1, C2 and C3). The selection was based on cophenetic and residual sum of squares (rss) (Figure S1).

2.3. Comparison of Immune Scores between Clusters

Using the Microenvironment Cell Populations (MCP) counter [26], we compared the immune scores among CD8+ T cells, cytotoxic lymphocytes, B cells, neutrophils, monocytic cells, myeloid dendritic cells, endothelial cells and fibroblasts between C1, C2 and C3.

2.4. Sample Preparation

The 347 TCGA samples were divided into training and testing cohorts with the caret package, which is a standard tool in building a prediction model [30]. This package focuses on simplifying model training and tuning across a wide variety of modeling techniques. It also includes methods for preprocessing training data, calculating variable importance and model visualizations. To prevent the bias of random allocation from undermining the stability of the subsequent modeling, all samples were put back into random groups 100 times in advance [31]. Herein, the group sampling of training and testing cohorts were performed in a ratio of 7:3. The most suitable training and testing cohorts were selected according to the following conditions: the two cohorts were similar in age distribution, FIGO stage and follow-up time. The gene expression profiles of the two randomly grouped cohorts were similar in the number of classified samples.

2.5. Lasso Regression Analysis

We further used lasso Cox regression to reduce the number of genes in the risk model. The lasso method is a regularization estimation used to build a more refined model by constructing a penalty function, thereby compressing some coefficients and setting some coefficients to zero [32]. When applying the glmnet package for lasso Cox analysis, we used 10-fold cross-validation for the model construction and analyzed the confidence intervals (CIs) in each lambda [33].

2.6. Construction of Nomogram Combined with Risk Score (RS) and Clinical Features

A nomogram is a method to display the results of the risk model intuitively and effectively, conveniently applied in prediction of the outcome [34]. It uses the length of the scale to represent different variables (RS, clinical features), thereby exhibiting the effect of their values on the outcome. We used TCGA cohort to build a nomogram that combined different prognostic variables.

2.7. Prediction Model Evaluation

To compare more than two groups, a Kruskal–Wallis test and one-way ANOVA were used as nonparametric and parametric tests, respectively. The Kaplan–Meier (KM) method was used to calculate the overall survival (OS) and a log-rank test determined

the significance. The clinical utility of the prognostic model was evaluated based on the receiver operating characteristic (ROC) curve and decision curve analysis (DCA). We used the concordance index (C-index) to compare the prediction performance between different models. All statistical analyses utilized R software (version 3.6.1).

2.8. Immunotherapy Prediction

To predict the response to immunotherapy, we selected the IMvigor 210 cohort with urogenital cancer patients who received a programmed death ligand 1 (PD-L1) blocking therapy [35]. The IMvigor210CoreBiologies package was used to extract clinical information and gene expression profile information, which were converted from counts to transcripts per million and further log2 processed. This cohort consists of 348 samples, including 232 deaths and 116 censored. After PD-L1 treatment, samples were classified into the following categories according to the patient's response: complete response (CR), partial response (PR), stable disease (SD) and progressive disease (PD). Among them, CR and PR are recognized as patients who respond to immunotherapy. SD and PD are recognized as patients who do not respond to immunotherapy. The value for the neoantigen (NEO) and the tumor mutation burden (TMB) of each sample is also given in this cohort. For further details, please refer to Table S2.

3. Results

3.1. Immune Scores Indicate Different Patterns According to Molecular Subtypes in OC

There were 347 OC samples from TCGA and 93 from the ICGC after preprocessing (Table 1). In the expression matrix of the whole TCGA cohort with 4061 genes, 87 prognostic TME-related genes ($p < 0.01$) were obtained by univariable Cox analysis (Table S3). Out of these genes, three clusters were built using NMF as described in Section 2.2. TCGA-OC samples were than divided into three clusters: C1, C2 and C3 (Figure 1a). Comparison of OS and progression-free survival (PFS) between the three clusters showed significant differences (Figure 1b–g). The majority of the immune scores, including CD8+ T cells, cytotoxic lymphocytes, B cells, neutrophils, monocytic cells, myeloid dendritic cells, endothelial cells and fibroblasts, revealed significant differences among the subtypes as well (Figure 1h–o).

Table 1. Sample information from The Cancer Genome Atlas (TCGA) and International Cancer Genome Consortium (ICGC) Australian ovarian cancer (OC) cohort.

Clinical Feature		TCGA	ICGC-Australian
Event	Censored	125	19
	Dead	222	74
FIGO stage	III	290	79
	IV	57	14
Grade	G1	1	
	G2	35	
	G3	302	
	G4	1	
	None	8	
Chemotherapy	Yes	322	
	No	25	
Recurrence	Yes	186	
	No	161	
Age	≤60	192	
	>60	155	
Residual disease	No	55	
	1–10 mm	25	
	11–20 mm	164	
	>20 mm	69	
	Unknown	34	

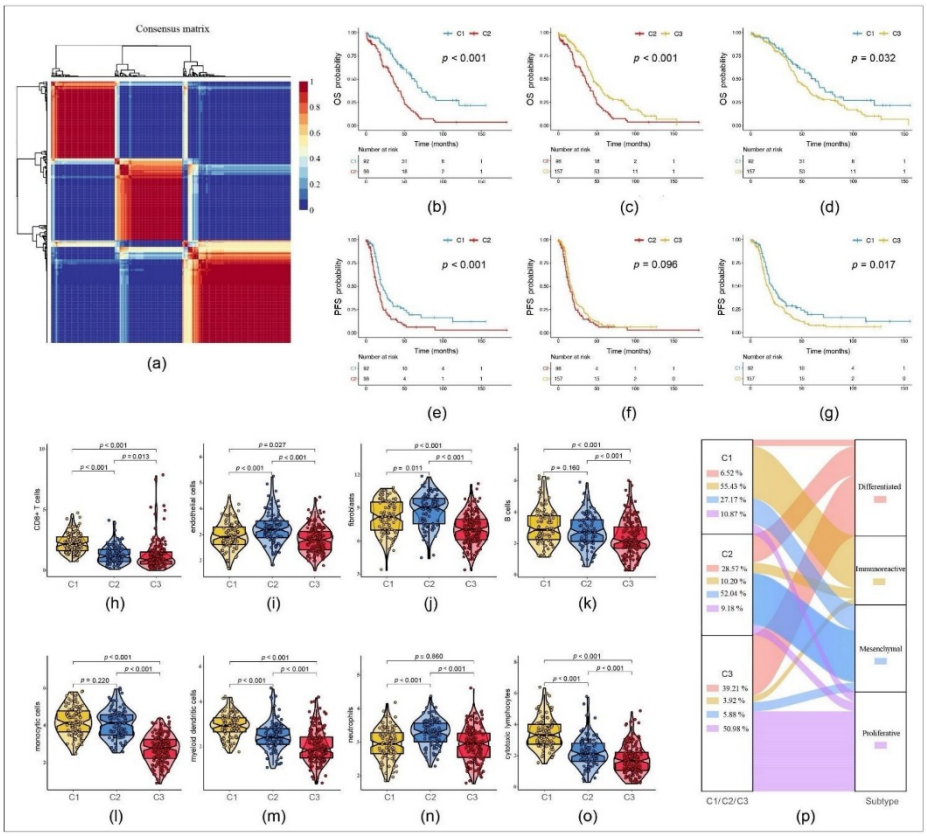

Figure 1. Comparison of the three clusters 1, 2 and 3 (C1, C2 and C3): (**a**) Consensus map clustered via the non-negative matrix factorization (NMF) algorithm. (**b**–**g**) Overall survival (OS) and progression-free survival (PFS) showed significant differences. (**h**–**o**) Immune scores of cells of the tumor microenvironment (TME) showed significant differences. (**p**) Percentage of the four molecular subtypes accounting for each of the three clusters.

According to TCGA research network, SOC can be divided into four molecular subtypes according to their expression of mRNA: differentiated, immunoreactive, mesenchymal and proliferative [36]. While these subtypes are based on the expression of all genes from TME and OC cells, our three clusters model included exclusively TME-related genes. When comparing C1, C2 and C3 with the existing TCGA classification based on the typing of all genes, we found that the immunoreactive subtype accounted for 55.43% of C1, mesenchymal subtype for 52.04% of C2 and proliferative subtype for 50.98% of C3 (Figure 1p).

3.2. Establishment of a Predictive RS Based on TME-Related Genes

The training cohort was composed of 243 samples and the testing cohort of 104 samples (Table 2). The results of the chi-squared test showed no significant differences in FIGO stage, grade, chemotherapy and recurrence status between them ($p > 0.05$), which confirmed the success of randomization.

Table 2. Comparison of TCGA training and testing cohort.

Clinical Feature		TCGA Training Cohort	TCGA Testing Cohort	*p*-Value
Event	Censored	92	33	0.3333
	Dead	151	71	
FIGO stage	III	201	89	0.6165
	IV	42	15	
Grade	G1	1	0	0.5779
	G2	22	13	
	G3	212	90	
	G4	1	0	
	None	7	1	
Chemotherapy	Yes	227	95	0.6481
	No	16	9	
Recurrence	Yes	128	58	0.6803
	No	115	46	
Age	≤60	140	52	0.1913
	>60	103	52	
Residual disease	No	41	14	0.8823
	1–10 mm	114	50	
	11–20 mm	17	8	
	>20 mm	46	23	
	Unknown	25	9	

The univariable Cox proportional hazard regression was conducted on the training cohort using the survival coxph function. Ninety-two prognostic TME-related genes were subsequently identified within the threshold of $p < 0.01$ (Table S4). The glmnet package [33] was used to further narrow the range of genes, while still maintaining high accuracy. From the change trajectory of independent variables, we can see that as lambda gradually decreased, the number of independent variable coefficients tending towards zero gradually increased (Figure S2a). We used 10-fold cross-validation to build the model and to analyze the CI under each lambda. We saw that the model performance was best when lambda was −2.8700 (Figure S2b). For this reason, we selected 24 genes according to the minimum lambda = 0.0566 as candidate genes. The Akaike information criterion algorithm was used to reduce the number of genes further and, finally, 11 genes were obtained, constructing this formula:

$$\begin{aligned}\text{risk score (RS)} = {} & -(5.9449 \times \textit{SNRPA1}) \\ & - (6.9887 \times \textit{CCL19}) \\ & - (4.4685 \times \textit{CXCL11}) \\ & - (6.9226 \times \textit{CDC5L}) \\ & - (6.1777 \times \textit{APCDD1}) \\ & - (8.9229 \times \textit{LPAR2}) \\ & + (0.2541 \times \textit{PI3}) \\ & + (1.7480 \times \textit{PLEKHF1}) \\ & + (5.4819 \times \textit{CCDC80}) \\ & + (0.3243 \times \textit{CPXM1}) \\ & + (0.7416 \times \textit{CTAG2}).\end{aligned}$$

The p-ROC package was used to analyze the prognostic classification effect of the RS in the training cohort. The 5-year ROC of the model was 0.78. According to the expression of the RS, we were able to divide the samples into a high-risk group (HRG) and a low-risk group (LRG) with the median as our cut-off.

A KM survival analysis showed that the prognosis of the HRG was significantly poorer than that of the LRG (Figure 2a). To validate the accuracy of our model, we applied

the same analysis on TCGA testing cohort, the entire TCGA cohort (TCGA training and testing cohort taken together) and the Australian ICGC cohort (Figure 2b–d). All KM curves showed a significant difference between the HRG and the LRG. In the three TCGA cohorts, the 5-year AUCs of the model were 0.78, 0.78 and 0.77. In the ICGC cohort, the 1-year AUC was 0.73. Meanwhile, the 3-year and 5-year AUCs were 0.59, partly because the median follow-up time used by the ICGC was shorter than the one used by TCGA.

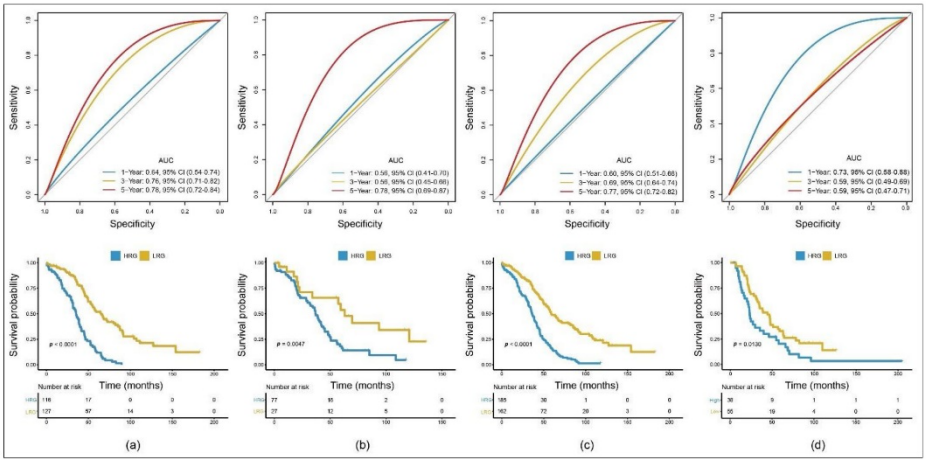

Figure 2. Construction and validation of the TME-related 11-gene risk score (RS) for serous ovarian cancer (SOC) with 1-, 3- and 5-year receiver operating characteristic (ROC) and OS Kaplan–Meier (KM) curves within the different cohorts: (**a**) TCGA training cohort; (**b**) TCGA testing cohort; (**c**) entire TCGA cohort; (**d**) Australian ICGC cohort.

3.3. RS Assessment in Subgoups Presenting Different Clinical Features or Mutation Statuses

Further, we categorized patient subgroups by age (≤60 years and >60 years), FIGO stage (III, IV), recurrence and chemotherapy status. In addition, we divided the samples into the HRG and LRG based on the already mentioned RS. In most cases, we found a significant difference in the prognosis between the HRG and the LRG (Figure 3a–g). Only the no chemotherapy status showed no significant difference in OS between both groups (Figure 3h). Our data indicate that our prediction model is able to predict OS according to age, FIGO stage III and IV, recurrence and chemotherapy status.

We then extracted the mutation status from all TCGA OC exon sequencing samples. Our aim was to verify whether our model could apply to different mutations as identified by TCGA. More specifically, *TP53*, *TTN*, *MUC16* and *CSMD3*, genes with the highest mutation frequency in OC, were included (Figure S3). For our TCGA cohort, we identified mutation status in 250 samples (in 97 samples the mutation status was unclear). All subgroups confirmed significant differences in the OS between the HRG and the LRG (Figure 3i,k,l,n–p). The subgroup without a *TP53* mutation and the one with a *MUC16* mutation showed no significance (Figure 3j,m).

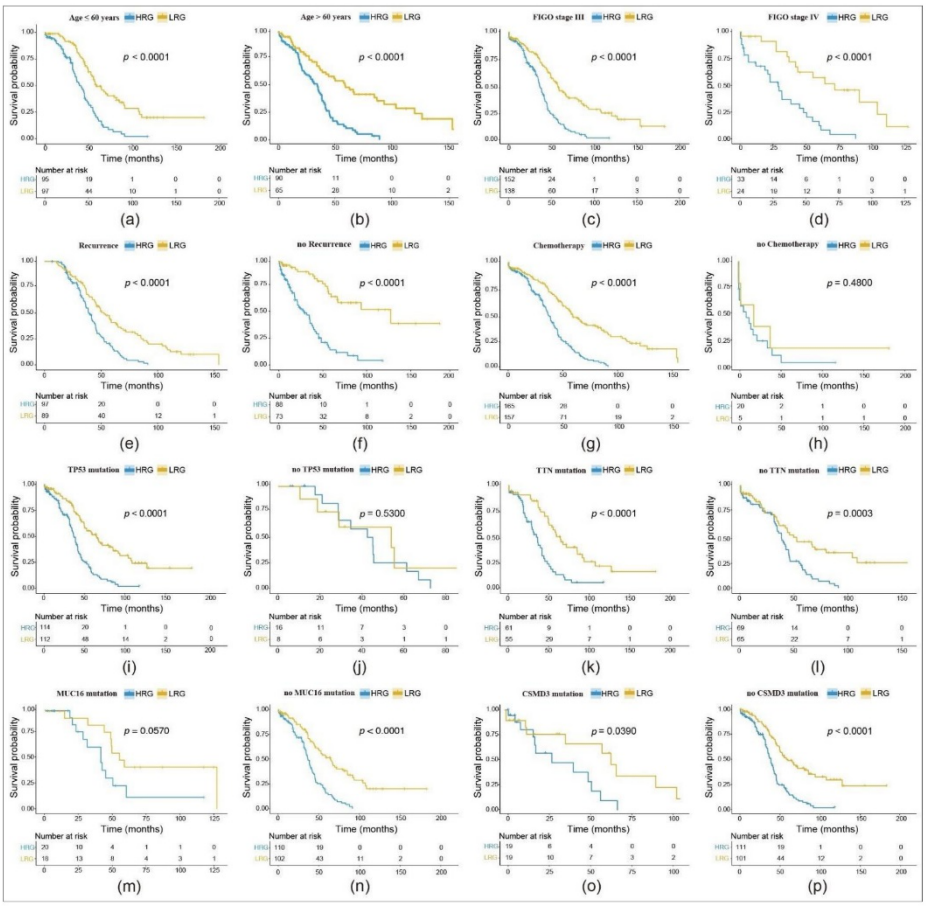

Figure 3. Evaluation of the 11-gene risk model in different subgroups with OS KM curves comparing the high-risk group (HRG) and the low-risk group (LRG): (**a**–**h**) Subgroups with different clinical features; (**i**–**p**) subgroups with different mutations.

3.4. TME-Related Genes Correlate with Clinical Outcome

We next employed univariable and multivariable Cox regression to analyze the relationship between RS and OS (Table 3). Our analysis revealed that RS is an independent risk factor with a hazard ratio (HR) of 2.499. A similar result was indicated by residual disease (HR = 1.70). In contrast, chemotherapy is an independent protective factor (HR = 0.35). FIGO stage, grade and recurrence showed no significance.

Consequently, we constructed a nomogram model including residual disease, RS and chemotherapy status. It showed that RS had the greatest impact on the prediction of survival rate (Figure 4a). Calibration plots visualized the 3-year and 5-year performance and showed that our nomogram is close to the 45° line that represents the optimum in prediction [37] (Figure 4b). In the 3-year ROC curve, the AUC of the nomogram was larger than other clinical variables, which can be seen in Figure 4c. However, in the 5-year ROC curve, the RS exceeded the nomogram and had the largest AUC (Figure 4d). Further, we

used DCA to evaluate the effectiveness of the model [38]. The standardized net benefit confirmed the 3-year predictive value in OS of the nomogram (Figure 4e) and the 5-year predictive value in OS of the RS (Figure 4f) when compared using a single clinical variable.

Table 3. Univariable and multivariable Cox regression to analyze the relationship between the RS and clinical prognosis.

Variables	Univariable Analysis			Multivariable Analysis		
	HR	95% CI	*p*-Value	HR	95% CI	*p*-Value
FIGO stage	1.16	0.82–1.66	0.408	1.24	0.86–1.78	0.251
Grade	1.03	0.67–1.58	0.884	1.12	0.73–1.71	0.620
Chemotherapy	0.29	0.18–0.48	<0.001	0.35	0.20–0.59	<0.001
Recurrence	1.15	0.86–1.54	0.353	1.21	0.89–1.65	0.227
Age	0.79	0.60–1.04	0.097	0.79	0.59–1.05	0.101
Residual disease	2.06	1.29–3.26	0.001	1.70	1.06–2.73	0.027
RS	2.19	1.53–3.15	<0.001	1.73	1.17–2.55	<0.006

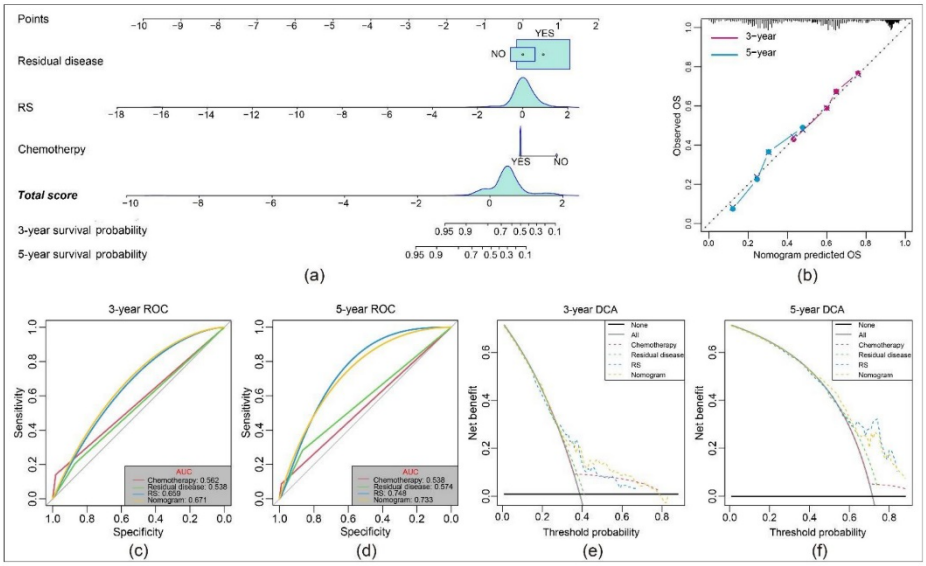

Figure 4. Clinical value of the predictive model: (**a**) Nomogram predicting the 3- and 5-year OS for patients. The points identified on the point scale of each variable are totaled. Finally, beneath the total points, the probability of 3- or 5-year survival is projected on the scales below. (**b**) Calibration curves for the nomogram predicted 3- and 5-year OS for patients in relation to actual survival. (**c**,**d**) ROC curves of the nomograms compared with other clinical variables. (**e**,**f**) Decision curve analysis (DCA) curves can evaluate the clinical benefit of the nomograms and their potential scope of application. Black indicates that all samples are negative and none are treated, therefore the net benefit is zero. Gray indicates that all samples are positive and all are treated. The x-axis represents the threshold probabilities.

3.5. The 11-Gene Signature Risk Model as a Novel Predictive RS in OC

To compare the prediction performance of our 11-gene signature with other models, we selected four other reported risk models: a 5-gene [39], an 8-gene [40], a 10-gene [41] and a 7-gene signature [42]. To make them comparable, we calculated the RS of each dataset using the same method (multivariable Cox regression analysis). In the validation of these results, we included the corresponding genes in these four models and then evaluated the ROC. The samples were subsequently divided into the HRG and the LRG according to the median RS value. The prognosis for the HRG and LRG was significant across all four models. However, the ROC curves showed a lower AUC, therefore, they were poorer in predicting the prognoses when compared to our model (Figure 5a–d).

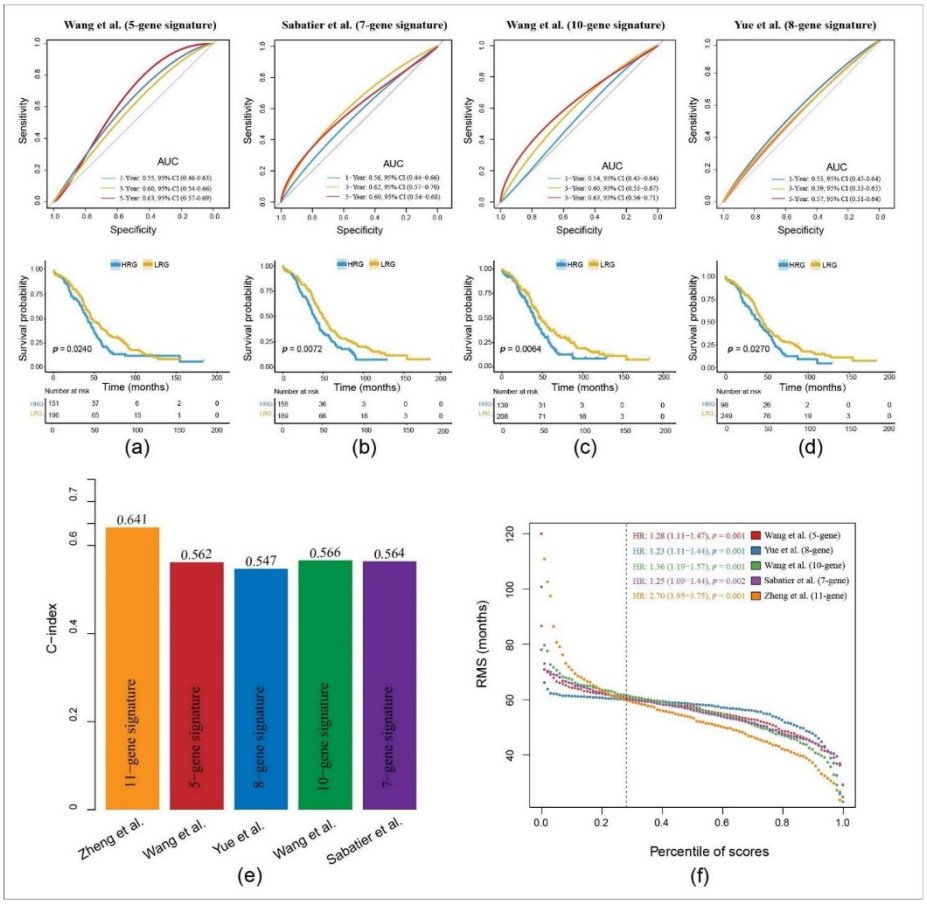

Figure 5. Comparison of the 11-gene risk model with other established models: (**a**–**d**) ROC and KM curves of four other published gene-signatures. (**e**) Concordance index (C-index) of the five prognostic risk models including our model, which has the highest C-index. (**f**) Restricted mean survival (RMS) time curve of all five prognostic risk models, revealing an overlap of 60 months.

The restricted mean survival (RMS) package was used to calculate the C-index of all prognostic signatures. Our model had the highest C-index with 0.641 (Figure 5e). With the RMS time, an evaluation of the predictive effect of the signatures at different time points was possible. As a result, our gene signature performed best at a time period greater than 60 months. This indicates that our model is not only suitable for predicting patient survival greater than five years, but is also the leading predictor at less than 60 months when compared with the other models (Figure 5f).

3.6. The 11-Gene Signature Risk Model Validation in Another Gynecological Cancer

We ran gene set enrichment analysis on samples within the HRG and LRG in order to show a possible over-proportional representation of essential signaling cascades. Thereby, we found the following immune and metabolism pathways with the associated normalized enrichment score (NES) and the adjusted *p*-value (*q*-value) enriched in the HRG (Figure 6a):

KEGG_PATHWAYS_IN_CANCER
(NES = 0.4600, q = 0.0049),
KEGG_T_CELL_RECEPTOR_SIGNALING_PATHWAY
(NES = 0.5604, q = 0.0030),
REACTOME_ADAPTIVE_IMMUNE_SYSTEM
(NES = 0.4685, q = 0.0010),
REACTOME_CYTOKINE_SIGNALING_IN_IMMUNE_SYSTEM
(NES = 0.4100, q = 0.0030),
REACTOME_METABOLISM_OF_LIPIDS
(NES = 0.4862, q = 0.0010).

Our analysis showed differences in the RS among OC subtypes as identified by TCGA [36]. More specifically, the RS was significantly higher in the mesenchymal subtype than in the differentiated, immunoreactive and proliferative subtypes. Moreover, the RS in the immunoreactive subtype was significantly lower than in the differentiated subtype. In conclusion, to a certain extent, our model is able to distinguish between the different molecular OC subtypes (Figure 6b).

Along with the pathway analysis in Figure 6a, we extracted the single gene expression of representative genes for generic pathway targets in gynecological oncology: immune checkpoints, DNA replication, mismatch repair and epithelial–mesenchymal transition (EMT). We then analyzed the correlation between the RS and these genes. RS was negatively correlated with immune checkpoint genes (*PDCD1*, *CD274* and *CTLA4*). In contrast, they were positively correlated with EMT-related genes (*FAP*, *TAGLN* and *LOXL2*) (Figure 6c).

To validate our 11-gene risk model in another gynecological cancer, we selected the cervical squamous cell carcinoma (CESC) cohort from TCGA. In this aim, our 11-gene RS was able to divide CESC samples into the HRG and LRG. The KM curve indicated that the prognosis of patients included in the HRG was significantly worse (p = 0.024) (Figure 6d).

Moreover, studies have shown that through the integration of genomic and proteomic characteristics, three molecular subtypes of cervical cancer can be distinguished. These are classified as the following: hormone, PI3K-AKT and EMT [43]. Given the predictive value of RS in OC molecular subtypes, the RS was able to differentiate among CESC subtypes: for the EMT subtype, the RS was significantly higher than the one obtained for the hormone subtype (Figure 6e).

We used the MCP counter and Estimation of Stromal and Immune cells in Malignant Tumor tissues using Expression data (ESTIMATE) to calculate different immune (cell) scores of the CESC samples and then calculated their correlation with the RS. It showed that the RS was negatively correlated with the stromal, immune and ESTIMATE score as well as with many immune and stromal cell lines (Figure 6f).

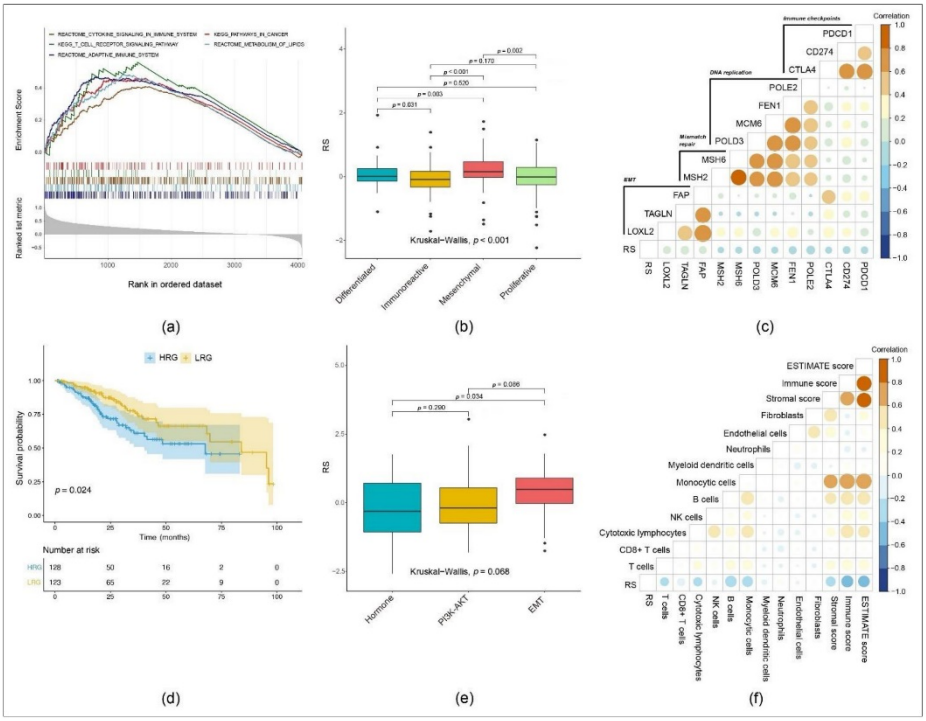

Figure 6. Functional analysis and pan-cancer verification of the model: (**a**) The main pathway groups overexpressed in the HRG. (**b**) RS comparison of the four molecular subtypes of TCGA OC. (**c**) Correlation between RS of OC samples and expression of representative genes for generic pathway targets in gynecological oncology (Pearson method). (**d**) OS of the HRG and the LRG in the KM curve when applying the 11-gene signature on the cervical squamous cell carcinoma (CESC) cohort. (**e**) RS comparison of the three molecular subtypes of TCGA CESC. (**f**) Correlation between RS of CESC samples and immune scores (Pearson method).

3.7. Prediction of Response to Immunotherapy Based on 11-Gene Risk Model

To date, immunotherapy does not play a major role in the therapy of OC [44,45]. However, new predictive biomarkers would be crucial for patient selection for immunotherapy. To explore whether our 11-gene model and subsequently the RS could predict the response to immunotherapy, we analyzed our immune signature in patients with urogenital cancer who received immunotherapy. We identified the IMvigor 210 cohort [35], which included gene expression and clinical responses from patients treated with PD-L1 blocking therapy. Comparing the HRG and LRG which were previously divided according to the RS, complete and partial immune responders accounted for 17.3% in the HRG and 27.3% in the LRG. Taken together, our results confirm the accuracy of the RS in another cancer entity (Figure 7a).

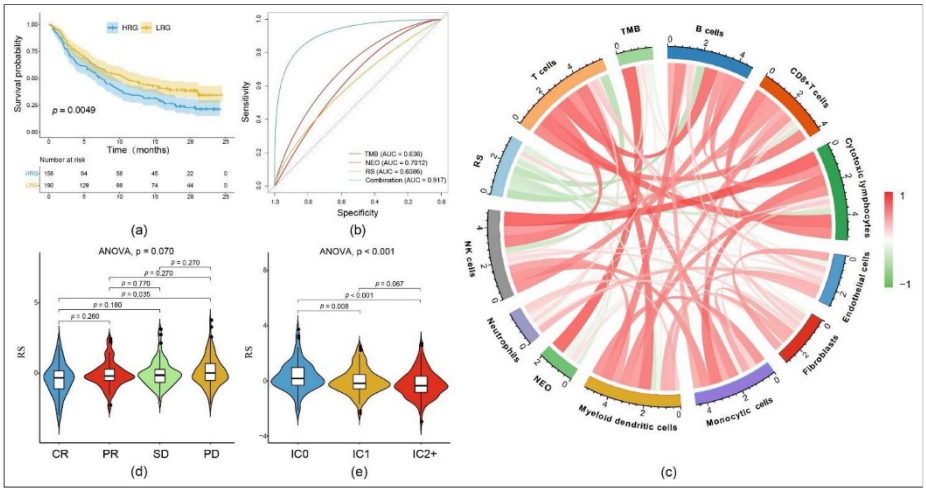

Figure 7. Prediction of potential immunotherapy using the RS in the IMvigor 210 cohort with human metastatic urothelial carcinoma samples from patients receiving programmed death ligand 1 (PD-L1) blocking immunotherapy: (**a**) The KM curve dividing the cohort into an HRG and an LRG according to the RS. (**b**) ROC curve for the prediction of treatment response to PD-L1 blocking therapy comparing tumor mutation burden (TMB), neoantigen (NEO), RS and the combination of all three. (**c**) Correlation between RS, immune cell score (IC-score), TMB and NEO. (**d**) RS according to the effectiveness of immunotherapy expressed as complete response (CR), partial response (PR), stable disease (SD) or progressive disease (PD). (**e**) RS according to different IC scores.

We combined our RS, the NEO and the TMB from the IMvigor 210 cohort [35] by logical regression to determine the treatment response and found that the AUC of this combination was as high as 91.7%. This is higher than both of the other single values: NEO (AUC = 0.701) and TMB (AUC = 0.636) (Figure 7b). We calculated the correlation between RS, NEO and TMB, as well as different immune scores using the MCP counter and found that the RS negatively correlated with all of them except fibroblasts (Figure 7c). Moreover, the RS showed significantly higher values ($p = 0.035$) in patients with PD compared to patients with CR. However, it was not able ($p > 0.05$) to distinguish between PR and SD (Figure 7d). Applying our RS to the IMvigor 210 cohort, we were able to significantly distinguish an immune cell score (IC score) of 0 from 1 ($p = 0.008$) as well as from 2+ ($p < 0.001$). The IC score categorizes tumors according to the percentage of PD-L1-positive immune cells (macrophages, dendritic cells and T cells): IC0 = 0%, IC1 < 5%, IC2+ $\geq$ 5%. In general, there was a significantly negative correlation between the RS and the IC score (Figure 7e). Additionally, an immunophenotypic analysis showed a low RS to be significantly associated with an immune inflamed phenotype (data not shown).

4. Discussion

The main finding of our study is the establishment of a powerful predictive model based on a TME-related gene signature in advanced-stage SOC.

As discussed in more detail below, we think it is crucial to explore prognostic markers given the TME's heterogeneity [46–48], to predict clinical response to targeted therapies.

In our study, 347 advanced-stage SOC samples and 4061 TME-related genes from TCGA were analyzed. We applied biostatistical methods to establish three molecular clusters. Additionally, immune scores, representing the proportion of several TME-related cell types, were compared between the clusters and showed significant differences. These

results were in line with the concept of a heterogeneous TME. Furthermore, correlation analyses with clinical parameters such as OS and PFS resulted in significant differences between these clusters as well.

In the present study, we showed that our 11-gene risk model (*SNRPA1*, *CCL19*, *CXCL11*, *CDC5L*, *APCDD1*, *LPAR2*, *PI3*, *PLEKHF1*, *CCDC80*, *CPXM1* and *CTAG2*) is able to indicate the prognosis of advanced-stage SOC patients. Previous studies investigated several genes, included in our signature, in an oncological context. For example, the mTOR pathway is able to participate in the malignant progression of hepatocellular carcinomas by activating *SNRPA1* [49]. In contrast, an elevated expression of *SNRPA1* would decrease our RS in OC patients. However, the role of *CTAG2*, coding for one of several tumor-associated autoantibodies that may have the ability to allow earlier diagnosis of SOC [50], is in line with our results. Even *CCL19*, transcribed by fibroblasts, inhibits the growth of lung cancer by promoting local anti-tumor T cell response [51] and *CXCL11* is known to be used as an enhancer of vaccine-induced CD8+ T cellular immunity [52].

The multivariable Cox regression analysis showed that the RS was an independent prognostic risk factor and remained robust when verified with internal and external cohorts. Next, we compared the HRG and LRG in defined subgroups, such as with or without a *TP53* mutation. While low-grade SOC is frequently characterized by *KRAS*, *BRAF*, *PTEN* and *CTNNB1* mutations, high-grade SOC expresses *TP53* mutations as its main molecular feature [53]. However, the correlation between *TP53*, the type of mutation and the prognosis of SOC is still controversial [54–57]. While our study is not able to close this gap in the knowledge, the RS showed a highly significant difference between the HRG and the LRG in the *TP53* mutated samples. Consequently, the RS can offer a resilient risk stratification in the huge group of high-grade SOC patients.

Nomograms are well established biostatistical methods in predicting the prognosis of patients with OC [58–62]. However, for the first time, we have constructed an advanced-stage SOC nomogram based on the TME-RS. ROC curve and DCA confirmed that the RS can accurately evaluate the prognosis of patients. When we compared our risk model to four other prognostic risk signatures from Wang et al. [39], Yue et al. [40], Wang et al. [41] and Sabatier et al. [42], our C-index demonstrated the highest AUC. These results indicate that the overall performance of our proposed model is superior to others. When we transferred this RS model to another gyneco-oncological entity, cervical cancer, it confirmed the ability to safely differentiate between the prognoses of an HRG and an LRG and between several molecular subtypes, all of which demonstrate potential pan-cancer usability.

Furthermore, our RS was strongly correlated with EMT-related genes. In contrast, immune checkpoints, DNA replication and mismatch repair were negatively correlated to the RS. Theoretically, a higher degree of immune infiltration in the LRG, partly represented through immune checkpoints, could account for greater immune defense capacity and consequently a better prognosis. Vice versa, the positively correlated EMT genes might cause OC's higher tendency to metastasize and a worse prognosis in the HRG.

In recent years, several clinical trials investigating immune checkpoint inhibitors in gynecological cancers were initiated and have attracted considerable attention [63]. Nevertheless, recently, study results on the PD-L1 inhibitors avelumab [44] and atezolizumab [45] revealed disappointing results in OC, as neither reached their primary endpoint of PFS. Additionally, for the programmed death 1 inhibitor pembrolizumab, we are still lacking encouraging phase III studies. This might be caused by the relatively small TMB in OC compared with other entities such as endometrial cancer [64]. Since immunotherapy gene datasets with clinical correlation for OC are not available, we selected another dataset which was obtained from samples of metastatic urothelial cancer treated with a PD-L1 blockade [35]. Hereby, our RS confirmed its performance in another cancer entity. Moreover, the accuracy of the prediction of a response to an anti-PD-L1 therapy is immensely increased by up to 91.7% if the RS is combined with NEO and TMB. This power is supported by the RS's ability to significantly differentiate CR from PD and distinguish between IC0 and IC1 as well as IC2+. Interestingly, our RS is negatively correlated with the PD-L1 expression,

which could be caused by a known phenomenon: "adaptive immune resistance" [65]. Here, when tumor cells are attacked by the immune system, interferon gamma is overexpressed through the active anti-tumor immune response. This induces the expression of PD-L1, indicating a strong attack by the immune system and in our case possibly leading to a better prognosis of the LRG patients [66,67]. The prognostic ability of our RS is supported through the correlation of a low RS with an immune inflamed phenotype, one of the three different phenotypes of immunology that most solid tumors exhibit [68]. Checkpoint inhibitors have already exerted anti-tumoral effects in this immunophenotype [69], which confirms our findings.

Of course, there are some limitations to this study. Firstly, as this is a retrospective study and interpatient variability is wide, and the results should be further verified in prospective studies. Secondly, all the SOC transcriptome data used were derived only from TCGA and ICGC databases. Lastly, estimations on the possible causality between gene expression and clinical findings, drawn in the discussion, need to be validated via further translational research trials. Hence, this unselected view on all TME-related genes was one of the initial aims of this study and can also be seen as a potential strength.

5. Conclusions

In conclusion, our study proposes a TME-related risk model to be implemented in the assessment of advanced-stage SOC patients. First, the accuracy of our RS to predict the biological response of cancer samples to an anti-PD-L1 immunotherapy could be clinically important. Even though several clinical trials failed to show a clinical benefit for checkpoint inhibition in OC patients [44,45], our RS might improve patient selection in future trials. Lastly, the establishment of a novel prognostic tool to predict a patient's prognosis based on an 11-gene signature might elevate prognostic accuracy, therefore encouraging users to combine several gene signatures. In this aim, the combination of this TME-related risk model with the gene signature based on lipid metabolism [70], which was recently published by our group, might be an option.

Supplementary Materials: The following are available online at https://www.mdpi.com/article/10.3390/cancers13133343/s1, Figure S1. Expression of prognostic TME-related genes between the three clusters: (a–c) Heatmaps comparing C1, C2 and C3. (d) The cophenetic correlation coefficient is used to reflect the stability of the cluster obtained from NMF. (e) rss is used to reflect the clustering performance of the model. Figure S2. Analysis of lasso regression: (a) Changing trajectory of each independent variable (the abscissa represents the corrected lambda and the ordinate represents the coefficient of the independent variable). (b) Log value of the independent variable lambda (the abscissa represents the CI of each lambda, and the ordinate represents errors in cross-validation). Figure S3. Distribution of common single nucleotide mutations in OC using TCGA biolinks package with 94.27% of samples altered. Table S1. The 4061 transcriptome-specific TME-related genes. Table S2. IMvigor 210 cohort. Table S3. The 87 prognostic TME-related genes from the entire TCGA cohort to establish C1, C2 and C3. Table S4. The 92 prognostic TME-related genes from TCGA training cohort to establish the RS.

Author Contributions: Conceptualization, M.Z., J.L., U.J. and T.K.; data curation, M.Z. and J.L.; formal analysis, M.Z., J.L. and T.K.; investigation, M.Z., J.L., A.C.-R., T.V., A.V., H.H.H., F.B., S.K. and T.K.; methodology, M.Z., J.L. and T.K.; project administration, U.J., F.T., S.M. and T.K.; resources, M.Z., J.L., A.C.-R., H.M. and T.K.; software, M.Z. and J.L.; supervision, U.J., F.T., S.M. and T.K.; validation, M.Z., J.L., A.C.-R., U.J. and T.K.; visualization, M.Z. and T.K.; writing—original draft, M.Z.; writing—review and editing, A.C.-R., H.M. and T.K. All authors have read and agreed to the published version of the manuscript.

Funding: We acknowledge financial support by the China Scholarship Council for Mingjun Zheng and by the Friedrich-Baur-Stiftung (registration number 33/19) for Till Kaltofen.

Institutional Review Board Statement: Not applicable.

Informed Consent Statement: Not applicable.

Data Availability Statement: Publicly available datasets were analyzed in this study and can be found here: https://www.cancer.gov/tcga and https://daco.icgc.org/ (accessed on 1 April 2021). Data generated by the authors are shown in this paper or in the Supplementary Material. Further data are available on request from the corresponding author, if they are not shown somewhere else.

Acknowledgments: The results shown here are in whole or part based upon data generated by TCGA (https://www.cancer.gov/tcga), ICGC (https://daco.icgc.org/) and ESTIMATE (https://bioinformatics.mdanderson.org/estimate/).

Conflicts of Interest: F.T.: Research support, advisory board, honoraria and travel expenses from AstraZeneca, Clovis, Medac, PharmaMar, Roche and Tesaro. S.M.: Research support, advisory board, honoraria and travel expenses from AbbVie, AstraZeneca, Clovis, Eisai, GlaxoSmithKline, Medac, MSD, Novartis, Olympus, PharmaMar, Pfizer, Roche, Sensor Kinesis, Teva and Tesaro. T.K.: Travel expenses from Roche. The funders had no role in the design of the study; in the collection, analyses, or interpretation of data; in the writing of the manuscript, or in the decision to publish the results. The other authors declare no conflict of interest.

Abbreviations

(*q*-value)	adjusted *p*-value
(CESC)	cervical squamous cell carcinoma
(CR)	complete response
(C-index)	concordance index
(CI)	confidence interval
(C1/2/3)	cluster 1/2/3
(DCA)	decision curve analysis
(EMT)	epithelial–mesenchymal transition
(ESTIMATE)	Estimation of Stromal and Immune cells in Malignant Tumor tissues using Expression data
(FIGO)	Fédération Internationale de Gynécologie et d'Obstétrique
(HR)	hazard ratio
(HRG)	high-risk group
(IC-score)	immune cell score
(ICGC)	International Cancer Genome Consortium
(KM)	Kaplan–Meier
(LRG)	low-risk group
(MCP)	Microenvironment Cell Populations
(NEO)	neoantigen
(NMF)	non-negative matrix factorization
(NES)	normalized enrichment score
(OC)	ovarian cancer
(OS)	overall survival
(PR)	partial response
(PD-L1)	programmed death ligand 1
(PFS)	progression-free survival
(PD)	progressive disease
(ROC)	receiver operating characteristic
(rss)	residual sum of squares
(RMS)	restricted mean survival
(RS)	risk score
(SOC)	serous ovarian cancer
(SD)	stable disease
(TCGA)	The Cancer Genome Atlas
(TME)	tumor microenvironment
(TMB)	tumor mutation burden

References

1. National Cancer Institute: Surveillance, Epidemiology, and End Results Program. Cancer Stat Facts: Ovarian Cancer. 2020. Available online: https://seer.cancer.gov/statfacts/html/ovary.html (accessed on 1 May 2021).
2. Waldmann, A.; Eisemann, N.; Katalinic, A. Epidemiology of Malignant Cervical, Corpus Uteri and Ovarian Tumours—Current Data and Epidemiological Trends. *Geburtshilfe Frauenheilkd* **2013**, *73*, 123–129. [CrossRef]
3. Menon, U.; Karpinskyj, C.; Gentry-Maharaj, A. Ovarian Cancer Prevention and Screening. *Obstet. Gynecol.* **2018**, *131*, 909–927. [CrossRef]
4. Mok, S.C.; Bonome, T.; Vathipadiekal, V.; Bell, A.; Johnson, M.E.; Wong, K.; Park, D.C.; Hao, K.; Yip, D.K.P.; Donninger, H.; et al. A gene signature predictive for outcome in advanced ovarian cancer identifies a survival factor: Microfibril-associated glycoprotein 2. *Cancer Cell* **2009**, *16*, 521–532. [CrossRef]
5. Lheureux, S.; Braunstein, M.; Oza, A.M. Epithelial ovarian cancer: Evolution of management in the era of precision medicine. *CA Cancer J. Clin.* **2019**, *69*, 280–304. [CrossRef] [PubMed]
6. Lorusso, D.; Ceni, V.; Daniele, G.; Salutari, V.; Pietragalla, A.; Muratore, M.; Nero, C.; Ciccarone, F.; Scambia, G. Newly diagnosed ovarian cancer: Which first-line treatment? *Cancer Treat. Rev.* **2020**, *91*, 102111. [CrossRef]
7. Kulbe, H.; Chakravarty, P.; Leinster, D.A.; Charles, K.A.; Kwong, J.; Thompson, R.G.; Coward, J.I.; Schioppa, T.; Robinson, S.C.; Gallagher, W.M.; et al. A dynamic inflammatory cytokine network in the human ovarian cancer microenvironment. *Cancer Res.* **2012**, *72*, 66–75. [CrossRef]
8. Reinartz, S.; Schumann, T.; Finkernagel, F.; Wortmann, A.; Jansen, J.M.; Meissner, W.; Krause, M.; Schwoerer, A.M.; Wagner, U.; Mueller-Bruesselbach, S.; et al. Mixed-polarization phenotype of ascites-associated macrophages in human ovarian carcinoma: Correlation of CD163 expression, cytokine levels and early relapse. *Int. J. Cancer* **2014**, *134*, 32–42. [CrossRef] [PubMed]
9. Hui, L.; Chen, Y. Tumor microenvironment: Sanctuary of the devil. *Cancer Lett.* **2015**, *368*, 7–13. [CrossRef]
10. Whiteside, T.L. The tumor microenvironment and its role in promoting tumor growth. *Oncogene* **2008**, *27*, 5904–5912. [CrossRef] [PubMed]
11. Nomelini, R.S.; Borges Junior, L.E.; de Lima, C.A.; Chiovato, A.F.C.; Micheli, D.C.; Tavares-Murta, B.M.; Murta, E.F.C. TNF-R2 in tumor microenvironment as prognostic factor in epithelial ovarian cancer. *Clin. Exp. Med.* **2018**, *18*, 547–554. [CrossRef]
12. Yin, M.; Li, X.; Tan, S.; Zhou, H.J.; Ji, W.; Bellone, S.; Xu, X.; Zhang, H.; Santin, A.D.; Lou, G.; et al. Tumor-associated macrophages drive spheroid formation during early transcoelomic metastasis of ovarian cancer. *J. Clin. Investig.* **2016**, *126*, 4157–4173. [CrossRef]
13. Pollard, J.W. Tumour-educated macrophages promote tumour progression and metastasis. *Nat. Rev. Cancer* **2004**, *4*, 71–78. [CrossRef]
14. Ma, Y.; Shurin, G.V.; Peiyuan, Z.; Shurinet, M.R. Dendritic cells in the cancer microenvironment. *J. Cancer* **2013**, *4*, 36–44. [CrossRef]
15. Feng, J.; Guo, J.; Zhao, P.; Shen, J.; Chai, B.; Wang, J. mTOR up-regulation of SNRPA1 contributes to hepatocellular carcinoma development. *Biosci. Rep.* **2020**, *40*, BSR20193815. [CrossRef] [PubMed]
16. Liu, J.F.; Herold, C.; Gray, K.P.; Penson, R.T.; Horowitz, N.; Konstantinopoulos, P.A.; Castro, C.M.; Hill, S.J.; Curtis, J.; Luo, W.; et al. Assessment of Combined Nivolumab and Bevacizumab in Relapsed Ovarian Cancer: A Phase 2 Clinical Trial. *JAMA Oncol.* **2019**, *5*, 1731–1738. [CrossRef]
17. Burger, R.A.; Brady, M.F.; Bookman, M.A.; Fleming, G.F.; Monk, B.J.; Huang, H.; Mannel, R.S.; Homesley, H.D.; Fowler, J.; Greer, B.E.; et al. Incorporation of bevacizumab in the primary treatment of ovarian cancer. *N. Engl. J. Med.* **2011**, *365*, 2473–2483. [CrossRef] [PubMed]
18. U.S. Food & Drug Administration. FDA Grants Accelerated Approval to New Treatment for Advanced Ovarian Cancer. 2016. Available online: https://www.fda.gov/news-events/press-announcements/fda-grants-accelerated-approval-new-treatment-advanced-ovarian-cancer (accessed on 1 May 2021).
19. Jimenez-Sanchez, A.; Memon, D.; Pourpe, S.; Veeraraghavan, H.; Li, Y.; Vargas, H.A.; Gill, M.B.; Park, K.J.; Zivanovic, O.; Konner, J.; et al. Heterogeneous Tumor-Immune Microenvironments among Differentially Growing Metastases in an Ovarian Cancer Patient. *Cell* **2017**, *170*, 927–938.e20. [CrossRef] [PubMed]
20. Tirosh, I.; Izar, B.; Prakadan, S.M.; Wadsworth, M.C.; Treacy, D.; Trombetta, J.J.; Rotem, A.; Rodman, C.; Lian, C.; Murphy, G.; et al. Dissecting the multicellular ecosystem of metastatic melanoma by single-cell RNA-seq. *Science* **2016**, *352*, 189–196. [CrossRef]
21. Rooney, M.S.; Shukla, S.A.; Wu, C.J.; Getz, G.; Hacohen, N. Molecular and genetic properties of tumors associated with local immune cytolytic activity. *Cell* **2015**, *160*, 48–61. [CrossRef] [PubMed]
22. Newman, A.M.; Liu, C.L.; Green, M.R.; Gentles, A.J.; Feng, W.; Xu, Y.; Hoang, C.D.; Diehn, M.; Alizadeh, A.A. Robust enumeration of cell subsets from tissue expression profiles. *Nat. Methods* **2015**, *12*, 453–457. [CrossRef]
23. Li, B.; Severson, E.; Pignon, J.C.; Zhao, H.; Li, T.; Novak, J.; Jiang, P.; Shen, H.; Aster, J.C.; Rodig, S.; et al. Comprehensive analyses of tumor immunity: Implications for cancer immunotherapy. *Genome Biol.* **2016**, *17*, 174. [CrossRef] [PubMed]
24. Chifman, J.; Pullikuth, A.; Chou, J.W.; Bedognetti, D.; Miller, L.D. Conservation of immune gene signatures in solid tumors and prognostic implications. *BMC Cancer* **2016**, *16*, 911. [CrossRef] [PubMed]
25. Aran, D.; Hu, Z.; Butte, A.J. xCell: Digitally portraying the tissue cellular heterogeneity landscape. *Genome Biol.* **2017**, *18*, 220. [CrossRef]

26. Becht, E.; Giraldo, N.A.; Lacroix, L.; Buttard, B.; Elarouci, N.; Petitprez, F.; Selves, J.; Laurent-Puig, P.; Sautès-Fridman, C.; Fridman, W.H.; et al. Estimating the population abundance of tissue-infiltrating immune and stromal cell populations using gene expression. *Genome Biol.* **2016**, *17*, 218. [CrossRef]
27. Andersen, P.K.; Grill, R.D. Cox's Regression Model for Counting Processes: A Large Sample Study. *Ann. Stat.* **1982**, *10*, 1100–1120. [CrossRef]
28. Therneau, T.M.; Grambsch, P.M. *Modeling Survival Data: Extending the Cox Model*; Springer: New York, NY, USA, 2013.
29. Gaujoux, R.; Seoighe, C. A flexible R package for nonnegative matrix factorization. *BMC Bioinform.* **2010**, *11*, 367. [CrossRef]
30. Kuhn, M. Building Predictive Models in R Using the caret Package. *J. Stat. Softw.* **2008**, *28*, 1–26. [CrossRef]
31. Breitung, K.; Ripley, B.D. Stochastic simulation. *Stat. Pap.* **1989**, *30*, 184. [CrossRef]
32. Tibshirani, R. Regression shrinkage and selection via the lasso: A retrospective. *J. R. Stat. Soc. Ser. B Stat. Methodol.* **2011**, *73*, 273–282. [CrossRef]
33. Friedman, J.; Hastie, T.; Tibshirani, R. Regularization Paths for Generalized Linear Models via Coordinate Descent. *J. Stat. Softw.* **2010**, *33*, 1–22. [CrossRef]
34. Zhang, Z.; Kattan, M.W. Drawing Nomograms with R: Applications to categorical outcome and survival data. *Ann. Transl. Med.* **2017**, *5*, 211. [CrossRef]
35. Cancer Genome Atlas Research Network. Integrated genomic analyses of ovarian carcinoma. *Nature* **2011**, *474*, 609–615. [CrossRef]
36. He, C.; Zhang, Y.; Cai, Z.; Lin, X.; Li, S. Overall survival and cancer-specific survival in patients with surgically resected pancreatic head adenocarcinoma: A competing risk nomogram analysis. *J. Cancer* **2018**, *9*, 3156–3167. [CrossRef]
37. Vickers, A.J.; van Calster, B.; Steyerberg, E.W. A simple, step-by-step guide to interpreting decision curve analysis. *Diagn. Progn. Res.* **2019**, *3*, 18. [CrossRef]
38. Wang, R.; Ye, X.H.; Zhao, X.L.; Liu, J.L.; Zhang, C.Y. Development of a five-gene signature as a novel prognostic marker in ovarian cancer. *Neoplasma* **2019**, *66*, 343–349. [CrossRef] [PubMed]
39. Yue, H.; Wang, J.; Chen, R.; Hou, X.; Li, J.; Lu, X. Gene signature characteristic of elevated stromal infiltration and activation is associated with increased risk of hematogenous and lymphatic metastasis in serous ovarian cancer. *BMC Cancer* **2019**, *19*, 1266. [CrossRef] [PubMed]
40. Wang, L.; Wang, L.; Ma, L.; Liu, J.; Ma, S. Identifying Gene Signature for the Detection of Ovarian Cancer Based on the Achieved Related Genes. *Gynecol. Obstet. Investig.* **2017**, *82*, 361–370. [CrossRef] [PubMed]
41. Sabatier, R.; Finetti, P.; Bonensea, J.; Jacquemier, J.; Adelaide, J.; Lambaudie, E.; Viens, P.; Birnbaum, D.; Bertucci, F. A seven-gene prognostic model for platinum-treated ovarian carcinomas. *Br. J. Cancer* **2011**, *105*, 304–311. [CrossRef]
42. Cancer Genome Atlas Research Network. Integrated genomic and molecular characterization of cervical cancer. *Nature* **2017**, *543*, 378–384. [CrossRef]
43. Pujade-Lauraine, E.; Fujiwara, K.; Ledermann, J.A.; Oza, A.M.; Kristeleit, R.S.; Ray-Coquard, I.L.; Richardson, G.E.; Sessa, C.; Yonemori, K.; Banerjee, S. Avelumab alone or in combination with pegylated liposomal doxorubicin versus pegylated liposomal doxorubicin alone in platinum-resistant or refractory epithelial ovarian cancer: Primary and biomarker analysis of the phase III JAVELIN Ovarian 200 trial. *Gynecol. Oncol.* **2019**, *154* (Suppl. 1), 21–22. [CrossRef]
44. Moore, K.N.; Bookman, M.; Sehouli, J.; Miller, A.; Anderson, C.; Scambia, G.; Myers, T.; Taskiran, C.; Robison, K.; Maeenpaeae, J.; et al. Atezolizumab, Bevacizumab, and Chemotherapy for Newly Diagnosed Stage III or IV Ovarian Cancer: Placebo-Controlled Randomized Phase III Trial (IMagyn050/GOG 3015/ENGOT-OV39). *J. Clin. Oncol.* **2021**. online ahead of print. [CrossRef]
45. Rosenberg, J.E.; Hoffman-Censits, J.; Powles, T.; van der Heijden, M.S.; Balar, A.V.; Necchi, A.; Dawson, N.; O'Donnell, P.H.; Balmanoukian, A.; Loriot, Y.; et al. Atezolizumab in patients with locally advanced and metastatic urothelial carcinoma who have progressed following treatment with platinum-based chemotherapy: A single-arm, multicentre, phase 2 trial. *Lancet* **2016**, *387*, 1909–1920. [CrossRef]
46. Hanahan, D.; Coussens, L.M. Accessories to the crime: Functions of cells recruited to the tumor microenvironment. *Cancer Cell* **2012**, *21*, 309–322. [CrossRef]
47. Schulz, M.; Salamero-Boix, A.; Niesel, K.; Alekseeva, T.; Sevenich, L. Microenvironmental Regulation of Tumor Progression and Therapeutic Response in Brain Metastasis. *Front. Immunol.* **2019**, *10*, 1713. [CrossRef]
48. Hanahan, D.; Weinberg, R.A. Hallmarks of cancer: The next generation. *Cell* **2011**, *144*, 646–674. [CrossRef] [PubMed]
49. Tran Janco, J.M.; Lamichhane, P.; Karyampudi, L.; Knutson, K.L. Tumor-infiltrating dendritic cells in cancer pathogenesis. *J. Immunol.* **2015**, *194*, 2985–2991. [CrossRef]
50. Kaaks, R.; Fortner, R.T.; Husing, A.; Barrdahl, M.; Hopper, M.; Johnson, T.; Tjønneland, A.; Hansen, L.; Overvad, K.; Fournier, A.; et al. Tumor-associated autoantibodies as early detection markers for ovarian cancer? A prospective evaluation. *Int. J. Cancer* **2018**, *143*, 515–526. [CrossRef]
51. Cheng, H.W.; Onder, L.; Cupovic, J.; Boesch, M.; Novkovic, M.; Pikor, N.; Tarantino, I.; Rodriguez, R.; Schneider, T.; Jochum, W.; et al. CCL19-producing fibroblastic stromal cells restrain lung carcinoma growth by promoting local antitumor T-cell responses. *J. Allergy Clin. Immunol.* **2018**, *142*, 1257–1271.e4. [CrossRef] [PubMed]
52. Namkoong, H.; Song, M.Y.; Seo, Y.B.; Choi, D.H.; Kim, S.W.; Im, S.J.; Sung, Y.C.; Park, Y. Enhancement of antigen-specific CD8 T cell responses by co-delivery of Fc-fused CXCL11. *Vaccine* **2014**, *32*, 1205–1212. [CrossRef] [PubMed]

53. Kurman, R.J.; Visvanathan, K.; Roden, R.; Wu, T.C.; Shih, L. Early detection and treatment of ovarian cancer: Shifting from early stage to minimal volume of disease based on a new model of carcinogenesis. *Am. J. Obstet. Gynecol.* **2008**, *198*, 351–356. [CrossRef] [PubMed]
54. De Graeff, P.; Crijns, A.P.; Ten Hoor, K.A.; Klip, H.G.; Hollema, H.; Oien, K.; Bartlett, J.M.; Wisman, G.B.; de Bock, G.H.; de Vries, E.G.; et al. The ErbB signalling pathway: Protein expression and prognostic value in epithelial ovarian cancer. *Br. J. Cancer* **2008**, *99*, 341–349. [CrossRef]
55. Shahin, M.S.; Hughes, J.H.; Sood, A.K.; Buller, R.E. The prognostic significance of p53 tumor suppressor gene alterations in ovarian carcinoma. *Cancer* **2000**, *89*, 2006–2017. [CrossRef]
56. Ahmed, A.A.; Etemadmoghadam, D.; Temple, J.; Lynch, A.G.; Riad, M.; Sharma, R.; Stewart, C.; Fereday, S.; Caldas, C.; Defazio, A.; et al. Driver mutations in TP53 are ubiquitous in high grade serous carcinoma of the ovary. *J. Pathol.* **2010**, *221*, 49–56. [CrossRef] [PubMed]
57. Koebel, M.; Reuss, A.; du Bois, A.; Kommoss, S.; Kommoss, F.; Gao, D.; Kalloger, S.E.; Huntsman, D.G.; Gilks, C.B. The biological and clinical value of p53 expression in pelvic high-grade serous carcinomas. *J. Pathol.* **2010**, *222*, 191–198. [CrossRef]
58. Previs, R.A.; Bevis, K.S.; Huh, W.; Tillmanns, T.; Perry, L.; Moore, K.; Chapman, J.; McClung, C.; Kiet, T.; Java, J.; et al. A prognostic nomogram to predict overall survival in women with recurrent ovarian cancer treated with bevacizumab and chemotherapy. *Gynecol. Oncol.* **2014**, *132*, 531–536. [CrossRef]
59. Lee, C.K.; Simes, R.J.; Brown, C.; Gebski, V.; Pfisterer, J.; Swart, A.M.; Berton-Rigaud, D.; Plante, M.; Skeie-Jensen, T.; Vergote, I.; et al. A prognostic nomogram to predict overall survival in patients with platinum-sensitive recurrent ovarian cancer. *Ann. Oncol.* **2013**, *24*, 937–943. [CrossRef]
60. Rose, P.G.; Java, J.J.; Salani, R.; Geller, M.A.; Secord, A.A.; Tewari, K.S.; Bender, D.P.; Mutch, D.G.; Friedlander, M.L.; Van Le, L.; et al. Nomogram for Predicting Individual Survival After Recurrence of Advanced-Stage, High-Grade Ovarian Carcinoma. *Obstet. Gynecol.* **2019**, *133*, 245–254. [CrossRef]
61. van de Laar, R.; IntHout, J.; Van Gorp, T.; Verdonschot, S.; van Altena, A.M.; Gerestein, C.G.; Massuger, L.F.; Zusterzeel, P.L.; Kruitwagen, R.F. External validation of three prognostic models for overall survival in patients with advanced-stage epithelial ovarian cancer. *Br. J. Cancer* **2014**, *110*, 42–48. [CrossRef] [PubMed]
62. Lee, C.K.; Simes, R.J.; Brown, C.; Lord, S.; Wagner, U.; Plante, M.; Vergote, I.; Pisano, C.; Parma, G.; Burges, A.; et al. Prognostic nomogram to predict progression-free survival in patients with platinum-sensitive recurrent ovarian cancer. *Br. J. Cancer* **2011**, *105*, 1144–1150. [CrossRef] [PubMed]
63. Patel, S.A.; Minn, A.J. Combination Cancer Therapy with Immune Checkpoint Blockade: Mechanisms and Strategies. *Immunity* **2018**, *48*, 417–433. [CrossRef] [PubMed]
64. Alexandrov, L.B.; Nik-Zainal, S.; Wedge, D.C.; Aparicio, S.A.; Behjati, S.; Biankin, A.V.; Bignell, G.R.; Bolli, N.; Borg, A.; Børresen-Dale, A.L.; et al. Signatures of mutational processes in human cancer. *Nature* **2013**, *500*, 415–421. [CrossRef]
65. Sharma, P.; Hu-Lieskovan, S.; Wargo, J.A.; Ribas, A. Primary, Adaptive, and Acquired Resistance to Cancer Immunotherapy. *Cell* **2017**, *168*, 707–723. [CrossRef] [PubMed]
66. Ribas, A. Adaptive Immune Resistance: How Cancer Protects from Immune Attack. *Cancer Discov.* **2015**, *5*, 915–919. [CrossRef]
67. Koyama, S.; Akbay, E.A.; Li, Y.Y.; Herter-Sprie, G.S.; Buczkowski, K.A.; Richards, W.G.; Gandhi, L.; Redig, A.J.; Rodig, S.J.; Asahina, H.; et al. Adaptive resistance to therapeutic PD-1 blockade is associated with upregulation of alternative immune checkpoints. *Nat. Commun.* **2016**, *7*, 10501. [CrossRef] [PubMed]
68. Hegde, P.S.; Karanikas, V.; Evers, S. The Where, the When, and the How of Immune Monitoring for Cancer Immunotherapies in the Era of Checkpoint Inhibition. *Clin. Cancer Res.* **2016**, *22*, 1865–1874. [CrossRef]
69. Vento, J.; Mulgaonkar, A.; Woolford, L.; Nham, K.; Christie, A.; Bagrodia, A.; de Leon, A.D.; Hannan, R.; Bowman, I.; McKay, R.M.; et al. PD-L1 detection using 89Zr-atezolizumab immuno-PET in renal cell carcinoma tumorgrafts from a patient with favorable nivolumab response. *J. Immunother. Cancer* **2019**, *7*, 144. [CrossRef] [PubMed]
70. Zheng, M.; Mullikin, H.; Hester, A.; Czogalla, B.; Heidegger, H.; Vilsmaier, T.; Vattai, A.; Chelariu-Raicu, A.; Jeschke, U.; Trillsch, F.; et al. Prognostic Model for Serous Ovarian Carcinomas Based on Lipid Metabolism Expression Profile. *Int. J. Mol. Sci.* **2020**, *21*, 9169. [CrossRef]

7. Acknowledgements

Over the course of my research and writing this paper, I would like to express my thanks to all those who have helped me.

First, I would like to express my gratitude to Prof. Udo. Jeschke, PD Dr.med. Fabian and Dr. med. Till Kaltofen for the project design, guidance, and supervision.

Sincere gratitude should also go to all the co-authors and colleagues for their constructive comments and thank the funding from China Scholarship Council (CSC).

Finally, I would like to show my warm gratitude to my wife, Ms. Chen Yue, who gave me much encouragement and support during this period!